Development of a current-voltage amplifier for precision measurements of low-level photocurrent

Robin Ehrminger

TALLINN UNIVERSITY OF TECHNOLOGY

Department of Mechatronics

Chair of Quality Engineering and Metrology /MHT

Development of a current-voltage amplifier for precision measurements of low-level photocurrent

Voolu-pinge võimendi arendamine madalate fotovoolude täppismõõtmiseks

Master's Thesis

The author applies for
the academic degree
Master of Sciences in Engineering

Author:
Robin Ehrminger

Supervisor:
Researcher Andrei Pokatilov

Tallinn

2016

Title: Development of a current-voltage amplifier for precision measurements of low-level photocurrent

Author's declaration:

I hereby declare that this thesis is the result of my independent work.

On the basis of materials not previously applied for an academic degree.

All materials used in the work of other authors are provided with corresponding references.

The work was completed _____ guidance.

The author:

_____
Robin Ehrminger
20*th* of May 2016

The work meets the requirements for a master's work.

Supervisor:

_____
Researcher Andrei Pokatilov
20*th* of May 2016

Permit to defense

Curriculum defense superior

_____
Prof. Mart Tamre
20*th* of May 2016

TUT Department of Mechatronics
Chair of Quality Engineering and Metrology /MHT

MASTERS THESIS SHEET OF TASKS

Year: 2016 semester: summer

Student:	Robin Ehrminger, ID: 145147
Curricular:	Mechatronics
Speciality:	Mechatronics
Supervisor:	Researcher Andrei Pokatilov
Advisor:	Prof. Toomas Kübarsepp

MASTERS THESIS TOPIC:

(in english): Development of a current-voltage amplifier for precision measurements of low-level photocurrent
(in estonian): Voolu-pinge võimendi arendamine madalate fotovoolude täppismõõtmiseks
Thesis tasks to be completed and the timetable:

Nr.	Description of tasks	Timetable
1.	Overview of methods for low-level photocurrent measurements	01.03.2016
2.	Design of the measurement system for low-level photocurrent measurements	14.03.2016
3.	Design and realisation of the measuring device	11.04.2016
4.	Development of software for the measuring system	02.05.2016
5.	Test and validation of the developed measurement system	09.05.2016

Solved engineering and economic problems:
Study and realization of the measurement system for low-level current measurements, design of the measuring device, development of software for the measuring system, validation of the measuring system.
Additional comments and requirements: No
Language: English

Application is filed not later than: 12.02.2016
Deadline for submitting the theses: 20.05.2016

Student: _____ $20th$ of May 2016

Supervisor: _____ $20th$ of May 2016

Confidentiality requirements and other conditions of the company are formulated as a company official signed letter.

List of symbols

A	Gain
$1/f_{noise}$	Floor noise
a	Variable for the exponential regression
A_p	Active sensor surface
b	Variable for the exponential regression
β	Regression variable
β_0	Linear regression coefficient
$\beta 1$	Linear regression coefficient
C_{DA}	Dielectric capacitance
C_{ERC2}	Serial capacitance of the input resistor
C_{int}	Integrator capacitor
D	Kolmogorov Smirnov coefficient
Δt	Integration time
E	Expected value
e_i	Residual of the individual value
H_0	Null hypothesis
H_1	Other hypothesis
h_i	Individual weightings
i_{in}	Input current
$i_{in,max}$	Maximum input current
$i_{in,min}$	Minimum input current
K_s	Tuning constant
L_{ESL}	Serial equivalent inductance
L_{ESL2}	Equivalent series inductance
O_i	Number of Pearson chi-square samples
Q_p	Light intensity
r_{adj}	Adjusted residuals
R_{DA}	Dielectric memory resistance
R_{eq}	Individual residual
R_{ESR}	Equivalent resistance
r_i	Serial resistor leakage
R_L	Serial resistance of the current source
R_s	Regression coefficient
$R - square$	Last square regression
s	Robust variance
$\sigma_y(\tau)$	Allan deviation

$\sigma_y^2(\tau)$	Allan variance
S_p	Sensor sensitivity
τ	Sampling frequency
$\tau^{-1/2}$	White noise slope
u_i	Weighting coefficient
$v(t)$	Time dependent voltage output
v_o	Voltage output
v_{Ref}	Reference voltage source
W	Shapiro-Wilk coefficient
w_i	Individual weight
$\widehat{y_i}$	Expected value
x	Regression variable
χ^2	Pearson chi-squared coefficient
x_i	Linear regression variable
Y	Regression function
y	Exponential regression function
y_i	Individual regression function

List of abbreviations

AD	Analog to digital converter
BNC	Bayonet Neill-Concelman connector
CMOS	Complimentary Metal-oxide-semiconductor
DA	Dielectric absorption
DC	Direct current
DMM	Digital-multimeter
DSP	Digital signal processor
DUV	Deep ultra violet
Est.	Estimation
LED	Light emitting diode
MOSFET	Field-effect transistor
NIR	Near infra-red
NP0	Class of ceramics used for capacitors
PCB	Printed circuit board
PTFE	Polytetrafluoroethylene
RF	Radio frequency
SW	Switch
TLL	Trigger logic level

Foreword

In English:

The thesis presents a design and validation of a switched integrator for precise measurement of low current levels with the range from 100 pA to 10 nA. The switching sequence is based on the microcontroller ATmega328P, which was programmed in order to generate high stability. The objected linearity and precision in context of stability and repeatability was measured with a stable reference current source. The stability effects of the current source and the parasitic effects of the integrating capacitor were investigated. The Allan deviation and the time based residual analysis were used in order to determine the characteristic noise floor of $4 * 10^{-6}$ V and the precision of the integrator. The performance of the switched integrator regarding the corrected non-linearity was below $0,06$ % over the expanded current range down to 100 pA. The precision in context of repeatability was found to be below $0,5$ % over the expanded range from 100 pA to 10 nA.

In Estonian:

Käesolevas uurimistöös on kirjeldatud kommuteeriva voolu-pinge võimendi ülesehitust ja valideerimist madalate voolude täppismõõtmisteks piirkonnas 100 pA kuni 10 nA. Seadme lülitusjada põhineb mikrokontrolleril ATmega328P, mis on programmeeritud kõrge stabiilsuse tagamiseks. Võimendi lineaarsust, stabiilsust ja korratavust mõõdeti stabiilse voolu tugiallikaga. Töös uuriti vooluallika stabiilsuse ja kommuteeriva kondensaatori parasiitefektide mõju võimendi toimivusele. Võimendi müarataseme ja täpsuse hindamiseks rakendati Allani hälbe ja ajadomeeni jääkvea meetodeid, karakteristlik müra väljatöötatud võimendile on $4 * 10^{-6}$ V. Võimendi karakteristliku ebalineaarsuse kompenseerimise järel saavutati toimimine madalate vooluväärtusteni kuni 100 pA tasemel $0,06$ %. Võimendi korratavuse hinnanguks saadi $0,5$ % voolupiirkonnas 100 pA 10 nA.

Contents

Chapter 1

Introduction

The Master's thesis is about a development of an analog integrator to measure low currents with high precision. The fully functional set-up is validated with all subcomponents. The subcomponents include different capacitor types and values as well as an approach to minimise parasitic effects in the measurement set-up.
The application of the integrator developed for the thesis is to measure extremely low power intensities (below 1 mW/m^2) with photodiodes. At such low power intensities the individual characteristics of photodiodes can be found and investigated.
The thesis consists of six chapters. After introducing the problem and objectives of the thesis the related work and the theoretical background are given. The experimental set-up, including the individual components selection process and the realisation, can be found in chapter 3. The following chapter 4 presents the measurement results together with the applied methods described in the theoretical part. The thesis ends with conclusion and summary.
This Master's thesis presents the results of joint activities between Metrosert AS and the Tallinn University of Technology.

1.1 Problem

The benefits of this work are connected with improving the measurement capability of low photocurrents. With the direct current measurement method the lowest input range of the DMM Agilent 3458A with the resolution of 1 pA is limited to 100 nA. By using the developed integrator of the current work, the reading rate of the multimeter can be increased from 3 sec. to $\sim$ 100 msec. The output rate of 3 sec. per reading limits the measurement capabilities in calibration of low power levels of photodiodes.

1.2 Objectives

The goal of the current thesis is to design and validate an analog integrator which converts currents into voltage output within the range of $0,2$ nA to 10 nA. The focus is on high gain levels of $\sim 10^9$ while linearity and precision in terms of stability and repeatability are considered as the mayor outcomes for validation.
The requirements to the switching integrator which is needed for calibration measurements can be found in the following table 1.1.

Parameter	Specification
Gain	$\sim 1 \times 10^9$
Integration time	1 ms to 1000 ms
Dynamic range	≈ 1 Hz
Linearity	$\leq \pm 1$ %
Precision	$\leq \pm 1$ %
User interface	LabVIEW

Table 1.1: Top level requirements for the integrator

In the thesis three hypotheses are tested.

Hypothesis 1: The stability of the switching sequence has direct impact on the integrator output stability.

Hypothesis 2: Non-linear effects increase with decreasing input current.

Hypothesis 3: Stability of the current source, parasitic effects and shielding against power line noise have a direct influence on precision and linearity of the integrator.

1.3 Related work

In general it is possible to divide the existing solutions into direct and indirect configurations. With the direct configuration the low current is measured directly with specialised devices, like nano-volt-meters, photon counters, photometer and several other devices.
The indirect method is to amplify and convert (to voltage) the low current signal before the measurement. Different amplifiers like transimpedance and capacitive feedback amplifiers have been applied to fulfil individual purposes like higher linearity or higher precision. In some cases these two amplifiers (transimpedance and integrators) are combined.
The devices for direct measurements are relatively expensive. An inexpensive way is so called "Bias Box" (in figure 1.1) which enables low current measurements with a gain from 1×10^2 up to 1×10^6 using a single resistor and a battery biased photo diode [8].

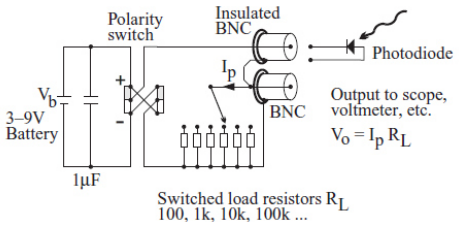

Figure 1.1: Low current "Bias Box" [8]

The analog integrator in general is applied in a wide range of applications. In this work five applications are presented. Switched integrators are most commonly found in applications for low power intensity measurements with photodiodes. In general high sensitive x-ray detectors use the switched integrator method to capture low level signals. The switched integrator can be found in optical roughness or cleanness measurements.
Another applications are analog PID controllers [2]. In material science integrators are used to measure leakage current of storage applications, for example batteries.

There are five scientific papers presented below. The papers are shortly summarised and similarities, differences, strengths and weaknesses related to this work are pointed out.

CMOS Circuit for LOW Photocurrent Measurements

[5]

Description: In this paper an ultra low current was measured by a two stage switched (by AD converter) CMOS amplifier. The main focus of this work is on noise reduction, non-linearity analysis and dark current calibration.
Similarities: Low current measurement with a switched amplifier stage
Differences: Two stage set-up, A/D converter for switching the circuits
Strengths: Relative precision of the A/D converter (five decades)
Weaknesses: No stability analysis

The CMOS circuit which was used in this paper is presented in figure 1.2.

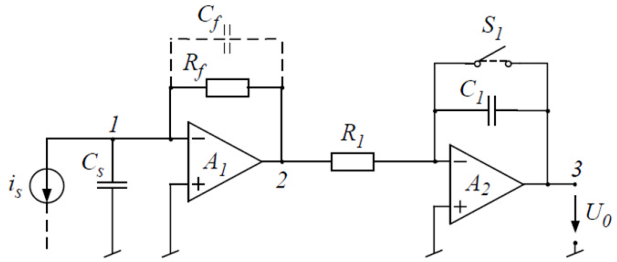

Figure 1.2: Transimpedance amplifier with sample-and-hold circuit [5]

Facility for fast Mapping of Total Scattering and Transmission in the Spectral Range from DUV- NIR

[9]

Description: The paper presents the quality analysis of optical surfaces with wide range detectors (from DUV to NIR range) in combination with capacitive feedback amplifiers.
Similarities: Integrator amplifier to measure the detector output with a multimeter, potential optical laboratory test set-up.
Differences: Specialised application regarding spectral analysis regarding transmission and scattering losses.
Strengths: Surface roughness analysis, contamination detection of optical surfaces
Weaknesses: Missing details about the detector-amplifier combination (not the main objective of the paper)

High performance optical absorbent detector based on low noise switched integrators

[10]

Description: This paper describes an experimental set-up to detect the absorption characteristics of liquids in a capillary flow cell. The spectral information was measured using a photodiode and an capacitive feedback amplifier combined with a LED light source.
Similarities: Switched integrating amplifier configuration (ACF2lOlBP-DIP), dynamic characteristics (Bandwidth).
Differences: LED light source, usage of an 2nd stage, amplifier, smaller pulse width (24sec), higher light source intensity.
Strengths: Linearity check and noise evaluation.
Weaknesses: Missing deviations of the reference and individual components, stability analysis for the set-up, comparison to a reference low current source.

The schematics of the switching integrator is presented in the following figure 1.3.

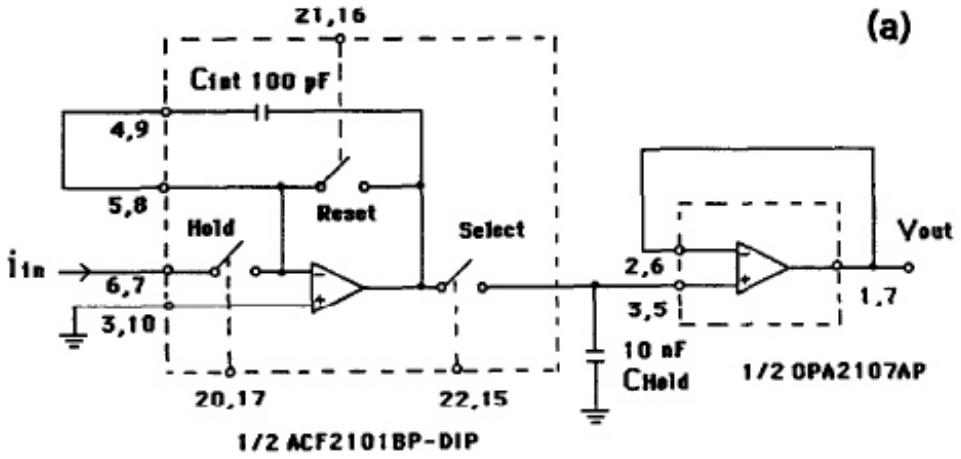

Figure 1.3: Switched integrator/sample-hold schematic [10]

Development of a switched integrator amplifier for high-accuracy optical measurements

[11]

Description: In this paper the main objective was to compare the capacitive feedback amplifier to the transimpedance configuration.
Similarities: Same precision integrated circuit and high gain
Differences: RS232 interface, 16 bit DSP for switching, 18 MHz counter clock
Strengths: Comparison of the amplifier types at high gain
Weaknesses: Low frequency response, slow signals, injection errors from solid-state

switches.

The integrator set-up is shown in figure 1.4.

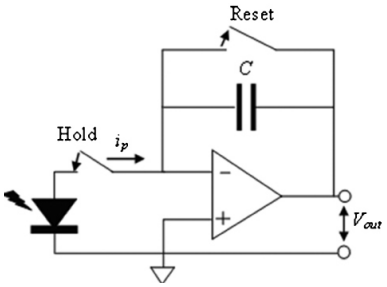

Figure 1.4: Switched integrator schematic [11]

Switched integration amplifier-based photocurrent meter for accurate spectral responsivity measurement of photometers

[13]

Description: This work presents a detailed comparison for different switched integrators with high gain of 10^7 and an input current range from 10 nA to 1 fA. These amplifiers are compared to each other regarding offset drift, integration time, uncertainty and spectral characteristics of different photometric standard diodes

Similarities: Switched integrator set-up for low current ranges.

Differences: Reed relay and driver for switching, different amplifiers with very low input current offset. Different output signal structure due to the use of one switch for reset.

Strengths: Analysis of amplifier characteristics due to stability, integration time, set-up validation due to thermal stability.

Weaknesses: Detailed analysis of the switching characteristics and influence of different capacitor types.

The set-up which was used in the paper can be found in the following figure 1.5.

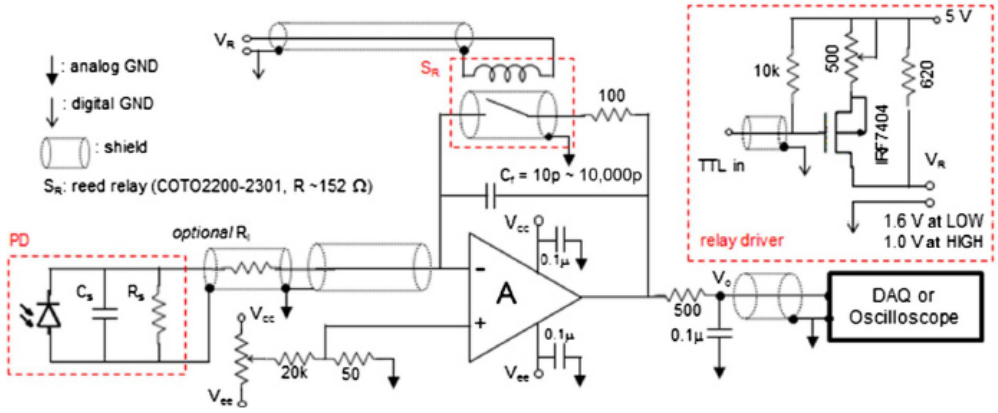

Figure 1.5: Switched integrator/sample-hold schematic [13]

Chapter 2

Theory

This chapter presents the ideal and "real" model of the integrator together with the current sources and their related equations.

2.1 Ideal integrator

The paper of Mountford [11] shows that the gain stability of the pure integrating op amps is better by the factor of two to three compared to the transimpedance amplifiers. Assuming that the capacitor is a purely reactive component, thermal noise is a non-existent [8].
The following figure 2.1 presents the switched integrator with the capacitance C_{int} and the photo current i_{in} [1]. A linear range without any parasitic effects is presented in the equations (2.1), (2.3). The equations show the linear relation between the input current i_{in} and the output voltage v_o as well as the gain.

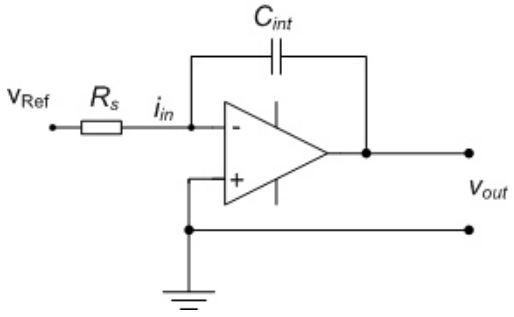

Figure 2.1: General capacitive feedback amplifier

$$v_{out}(t) = -\frac{1}{R_s C_{int}} v_{in}(t) \frac{d}{dt} \tag{2.1}$$

$$i_{in}(t) = C_{int} \frac{dv}{dt} \tag{2.2}$$

$$A = -\frac{dt}{C_{int}} \tag{2.3}$$

2.2 Model with imperfections of the integrator

Different capacitor types provide different storage capabilities. The systematic imperfections of the integration capacitor C_{int} are shown in the figure 2.2.

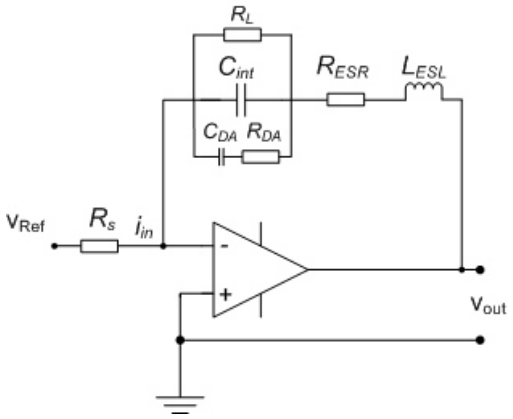

Figure 2.2: Imperfect capacitor model of the integrator

The main components which contribute to the overall leakage current of the imperfect capacitor are the parallel resistance R_L, the equivalent series resistance (R_{ESR}), the equivalent series inductance (L_{ESL}) and the dielectric absorption or memory (R_{DA}) [6].
The first component, the parallel resistance R_L is especially important regarding the leakage current of storage applications like integrators and capacitors in high impedance amplifiers. The ideal capacitor only responds to the current flow while the charge of "real" capacitors creeps through the isolation resistance *(ibid)*.
Secondly, the equivalent series resistance (R_{ESR}) of a capacitor describes the impedance of the capacitor plates which dissipates power while a currents are flowing. The contribution of this effect increases with dynamic of the current flow (e.g. RF applications and precision applications) *(ibid)*.
The third component, the equivalent series inductance (L_{ESL}) represents the inductance of the capacitor leads which are in series with the inductance of the capacitor plates. Similar to the series resistor this effect becomes important for higher frequency (RF) or precision applications *(ibid)*.

The dielectric absorption (C_{DA}) and (R_{DA}) models a similar effect to the hysteresis. An internal charge discharges and recovers some of its applied charge. As this effect depends on the previously applied charge it can be modelled as a charge memory effect. This error will appear for standard ceramic capacitors that are not specialised for charge storage *(ibid).*
The following equation represents the general behaviour of the integrator with imperfections including the voltage source drift $v_{in}(t)dt$ and the initial zero offset $v_0(t)$.

$$-v_{out}(t) = R_{eq} + R_{ESR} + L_{ESR}\frac{di_{in}}{dt} + (\frac{1}{C_{int}} + \frac{1}{C_{DA}})\int_{t0}^{t} v_{Ref}(t)dt + v_0(t) \tag{2.4}$$

with

$$R_{eq} = \frac{R_L R_{DA}}{R_L + R_{DA}} \tag{2.5}$$

2.3 Current source

For the ideal resistor the Ohm's law can be applied as in the following equation 2.6. In the figure 2.3 the ideal (a) and real current source (b) are presented.

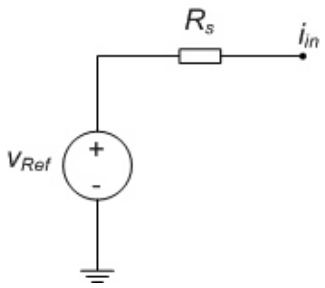

(a) Ideal current source

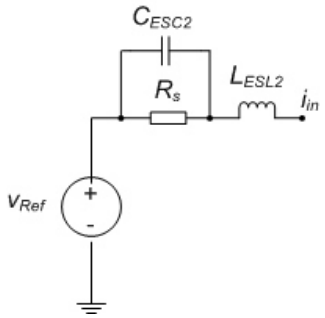

(b) Real current source

Figure 2.3: Current source with the ideal (a) and real (b) resistor

$$i_{in} = \frac{v_{Ref}}{R_S} \tag{2.6}$$

The real resistor with the introduced serial inductance L_{ESL2} and serial equivalent capacitance C_{ERC2} can be mathematical described like in the following equation.

$$i_{in}(t) = \frac{d^2V_{Ref}}{dt^2} + \frac{dV_{Ref}}{dt}\frac{1}{R_S C_{ESC2}} + L_{ESL2}\frac{di}{dt} \tag{2.7}$$

2.4 Allan deviation

The Allan deviation is a stochastic method based on serial correlation. It is used to determine the lowest possible standard deviation for the certain measurement time. In this thesis Allan deviation is used to characterise the precision considering white noise and floor noise.
In figure 2.4 the ideal slope $\tau^{-\frac{1}{2}}$ defines the range a.) of white noise while the floor noise $1/f_{noise}$ is marked with b.). The floor noise is a general characteristic of any device and it can be used for comparison of different components of one set-up. The time constant τ is defined by the sampling frequency and $Time$ describes the duration time of the measurement. The equation 2.9 shows two components in the nominator which are subtracted from each other. The $\bar{y}_{k+1}(\tau)$ represents the first half of the measurement series +1 sample depending on the time constant (sampling frequency τ). The $2nd$ part $\bar{y}_k(\tau)$ represents the $2nd$ half of the measured samples which depends also on τ. The result of the Allan deviation (equation 2.9) represents the mean squared difference. With the square root of the Allan deviation the Allan variance (equation 2.8) is obtained [3].

$$\sigma_y(\tau) = \sqrt{\sigma_y^2(\tau)} \tag{2.8}$$

and

$$\sigma_y^2(\tau) = \frac{[\bar{y}_{k+1}(\tau) - \bar{y}_k(\tau)]^2}{2} \tag{2.9}$$

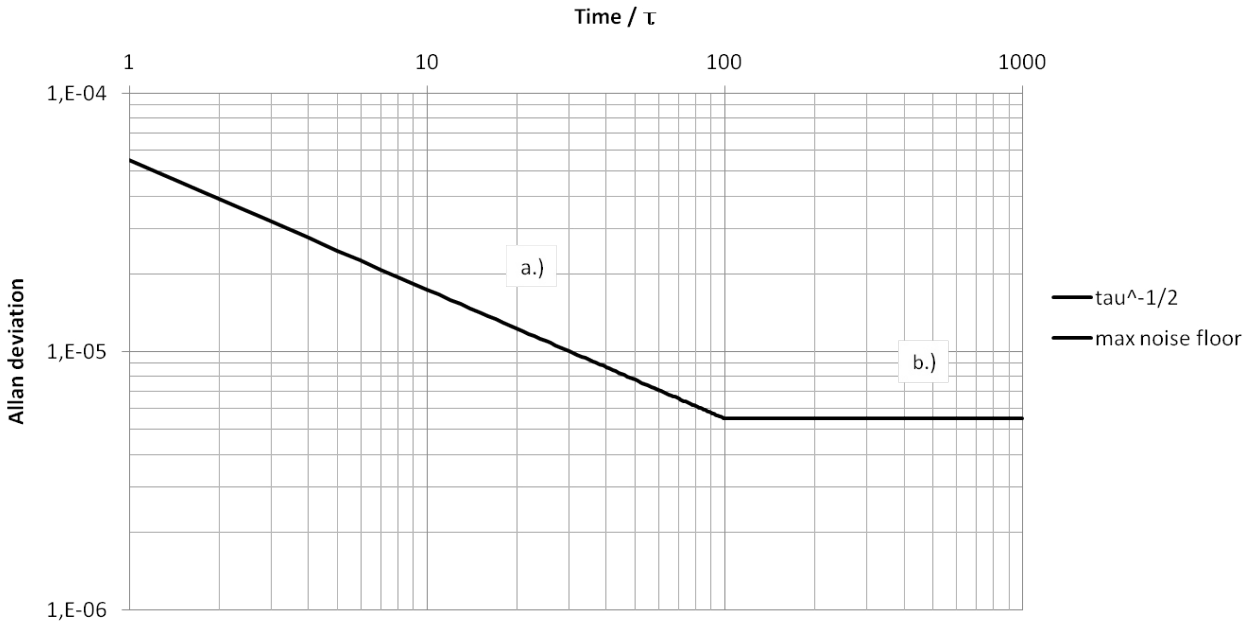

Figure 2.4: Noise level estimation with Allan deviation

2.5 Time series analysis

2.5.1 Residuals and linear regression

Residuals

For validation of the measurement results the residual analyses is used. This statistical method can be used to analyse partially linear drift problems by assuming that the drift problem is linear and the regression of Y on X is independent to the observations Y_1, ..., Y_n. Supposed that the data (x_i, e_i) for $i = 1, \ldots, n$ are plotted on one plane, the sum of residuals e, from 1 to n must be 0. To fulfil this criteria the residuals should be scattered randomly on positive and negative side. Positive residuals e_i tend to concentrate on the extreme or central values of x_i. The residual e_i in general is the result of the subtraction of the measured sample y_1 and the predicted value $\widehat{y}_i$ [4].

$$e_i = y_i - \widehat{y}_i \tag{2.10}$$

Regression

The general regression analysis is based on the dependent variable Y as a function of the independent variable X and the unknown parameter β.
The general form for any regression analysis is based in the expected value E and the following relation *(ibid)*.

$$Y \sim f(X, \beta) \tag{2.11}$$

$$E(Y/X) = f(X, \beta) \tag{2.12}$$

In case of linear regression the dependent variable y_i is a linear combination with the independent variable x_i together with the β_0 and $\beta 1$ parameters. With ϵ_i the individual error is described in the following equation 2.13 *(ibid)*.

$$y_i = \beta 0 + \beta_1 x_i + \epsilon_i \tag{2.13}$$

In case of non-linear regression the single component exponential function is generally solved by:

$$y = ax^b \tag{2.14}$$

which is non iteratively solved by

$$ln(y) = ln(a) + x \tag{2.15}$$

2.6 Algorithm for linearity correction

The general exponential equation to fit the relative deviation together with the bi-square robust regression algorithm is used to minimise the relative deviation of the integrator linearity.

2.6.1 Bi-square regression

The bi-square robust regression method minimises the weighted sum of squares, while the weight depends on the distance to the fitted line. The samples near the fit algorithm get the full weight while points farther from the fit get reduced weight. Points that are farther from the predicted line that would be expected by random chance are excluded. The robust regressing is build on the weighted last squares method (equation 2.16)[4].

$$s = \sum_{n=1}^{n} w_i (y_i - \widehat{y}_i)^2 \tag{2.16}$$

The coefficient w_i represents the weights. The weights describes the influence of the individual measured value to the parameter estimation. The smaller difference between the fit and real data indicates the higher quality which is supported by higher individual weights. The bi-square weights (equation 2.17) use an iterative algorithm which is based on the reweighed last-squares *(ibid).*

$$w_i = (1 - (u_i)^2)^2 \quad |u_i| < 1 \quad and \quad |u_i| \quad \geq 1 \tag{2.17}$$

with

$$u = \frac{r_{adj}}{K_s} \tag{2.18}$$

The variable K_s represents the tuning constant of $4,685$ and s is the robust variance given by MAD/0,6745 where MAD is the median of the absolute deviation of the residuals. To obtain the adjusted residuals r_{adj}, the individual residuals r_i are divided by the adjusted deviation of individual weightings h_i *(ibid).*

$$r_{adj} = \frac{r_i}{\sqrt{1 - h_i}} \tag{2.19}$$

2.7 Test of normality

The normal distribution has been thoroughly studied mainly for one reason. Measurement data often appears in form of the norm "bell-shaped" distribution. In metrology the normal

distribution is often used as a base for b-type uncertainty estimations. The obtained data can effect the properties of the normal distribution estimation or inferential methods which are used for data analysis. In order to ensure that the measurement data relays on the normal distribution several methods have been developed. Several statistical analysis methods are based on the assumption of the normal distributed samples [15].
Assuming the random number of independent samples n and identically distributed observations of the variable x appear in from of an unspecified density f(x). The general quality estimation of the fit is based on the null hypothesis H_0 (normal distribution) testing against another hypothesis H_1. Usually the mean (μ) and the standard deviation (σ) are unknown *(ibid)*.

$$H_0 : f(x) = \frac{1}{\sqrt{2\pi}\sigma} e^{\frac{-(x-\mu)^2}{2\sigma^2}} \tag{2.20}$$

$$H_1 : f(x) \neq f_0(x) \tag{2.21}$$

To evaluate the significance of the hypothesis test the p-value is generally used with the 5% criteria. For interpretation of the strength of evidence a p-value below 0,05 is seen as a strong evidence against the null hypothesis. In case of p-values close to the 0,05 criteria the observer decides individually *(ibid)*.

2.7.1 Shapiro-Wilk normality test

In general the Shapiro-Wilk normality test compares an estimate of the standard deviation by a linear combination between the statistical order and an estimation.
The Shapiro-Wilk normality test method provides the statistical coefficient W which is the result of a summed and factorised (a_i) input data (y_i) due to the variance (S^2). The mathematical relation can be found in the following equation [12].

$$W = \frac{\left(\sum_{n=1}^{n} a_i * y_i\right)^2}{n * S^2} \tag{2.22}$$

2.7.2 Kolmogorov-Smirnov test

In general the Kolmogorov-Smirnov test uses the cumulative distribution function to reduce the problem to one hypothesis test.
The test quantifies the deviation between the empirical distribution function $f_1(x)$ and reference distribution $f_0(x)$. The so called null hypothesis implies that the empirical data set is based on the normal distribution [12].

$$f_1(x) = \frac{1}{n}\sum_{n=1}^{n} I_{[-\inf,x]}(X_i) \tag{2.23}$$

with

$$I_{[-\inf,x]}(X_i) \tag{2.24}$$

$$D = sup|f_1(x) - f_0(x)| \tag{2.25}$$

2.7.3 Pearson chi-square normality test

The chi-square distribution is based on the so called gamma distributions. The gamma distributions appear as sampling distributions of variance estimators based on random samples which are situated on the normal distribution. The Pearson chi-square normality test is another method to analyse large data sets. This method compares the experimental data set with the χ^2 distribution [4].

$$\chi^2 = \sum_{n=1}^{n} \frac{(O_i - E_i)^2}{E_i} \tag{2.26}$$

with

χ^2: Defines the cumulative statistical Pearson's coefficient which approximates the Chi-square distribution asymptotically.
O_i: represents the number of samples ($type_i$)
E_i: defines the the theoretical periodic type.
n: covers the number of cells in the table.

2.8 Power intensity estimation

For the initial assessment a light intensity (Q_p) range for the designed integrator configuration is 0,1 to 3 $\frac{mW}{m^2}$. To detect this intensity level the properties of the photodiode S1337-33BR (Hamamatsu Photonics) are used for the initial estimation [7].

$$i_{in_{min}} = Q_p * A_p * S_p \tag{2.27}$$

with

Active sensor surface mm $A_p = 5,7\ mm^2$

Sensitivity in $S_p = 0,62\frac{A}{W}$

With the equation (2.27) the maximum $i_{in,max} = 10$ nA and the minimum current $i_{in,min} = 0,2$ nA for the integrator are defined.
In the following chapter the experimental set-up describes the individual parts and the component based pre evaluation. The estimated output range at the op amp gain of 10^9 is presented in the following table 2.1. With higher gain, higher output can be achieved.

Est. light intensity in $[mW/m^2]$	Est. photo current in $[nA]$	Est. Amplifier voltage output in $[V]$
3	10,3	-10,3
2	6,9	-6,9
1	3,5	-3,5
0,2	0,7	-0,7
0,05	0,17	-0,17

Table 2.1: Estimation of integrator output at the expected radiation intensity

Chapter 3

Experimental set-up

The experimental set-up, shown in figure 3.1, consists of three main objects: the integrator, digital multimeter with 6 $\frac{1}{2}$ digits (Agilent 34410A) and the Arduino.
The Arduino generates the pulse sequence to enable different modes on the switched integrator. The switching logic is based on the ATmel microcontroller (ATmega328) with the 16 MHz clock and 8 bit resolution which is used to get an highly stable pulse.
The programmed code is optimised regarding the pulse stability with synchronous switching capabilities. High level commands were tested with not successful results regarding stability and timing flexibility, so the register and port manipulation methods are used. The generated pulses are connected to the integrated MOSFET switches of the amplifier. The MOSFET switches define three sequences (integration, hold and reset) which are thoroughly described in the following sections.

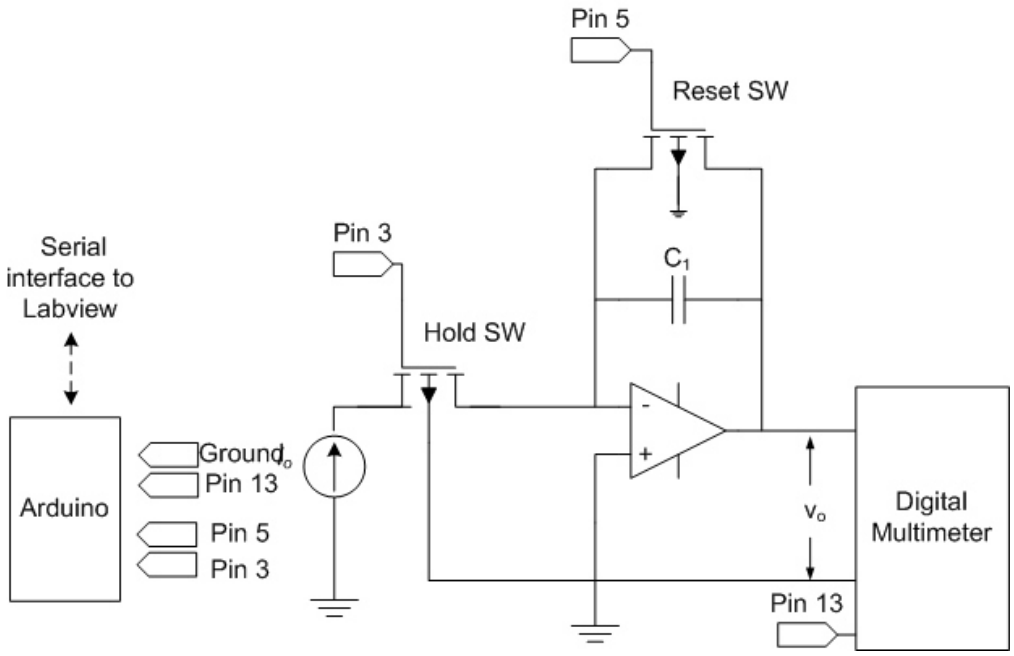

Figure 3.1: Experimental test set-up

3.1 Integrating amplifier

The low noise and switched integrator Burr Brown ACF2101BU ($\frac{1}{2}$ of the dual amplifier) was used. The choice was based mainly on many positive published results for the desired measurement range, its compact size, the low bias current of 100 fA and the high switch impedance of 1000 GΩ to minimise possible leakage. Additionally the integrator in general provides a relative low noise level of 10 μV_{RMS} with a wide dynamic range of 120 dB.
The integrator provides an internal capacitor as well as the option for an external capacitor which is used in this work.
In order to minimise the heat and the possible thermal side effects, the supply power was set to −15 V and +5 V. The ground design is in a star formation (single layer copper PCB) which was used as a carrier for all other components. The integration solution takes less room and provides an extra internal ground shield against stray capacitance. Furthermore it makes easier to integrate other components like the power supply capacitors and connectors [14].

3.2 Switching sequence

The integrator is used in the two switches configuration with the un-switched output *(ibid)*. With two switches the four different modes which are shown in figure 3.2 were programmed *(ibid)*.
The integration time (event from 1. to 2.) defines the time while the capacitor is charging. The hold mode (event 2. to 3.) keeps the maximum value (negative voltage) for measurements. Reset enables to start the same cycle from the same reference 0 V level. The 2nd hold after the reset (shown in event 5. to 6.) disconnects the input current. For long hold times $> 1\mu$s the internal leakage current will cause a voltage drop *(ibid)*. The real output after the integration is completed (event 2.) shows the internal leakage and the leakage charge of the integrating capacitor in form of a voltage "drop" or "drift" which depends on the capacitor type.
To provide the obligated accuracy and to take a partially stable reading with the digital multimeter the measurement time was reduced to its minimum. To make this possible the trigger (falling edge) was synchronised to the end of the integration time. The internal delays of the DMM (Agilent 34410A) with serial communication are specified with 2.9 ms. To ensure a stable reading the hold time was set to 5 ms.

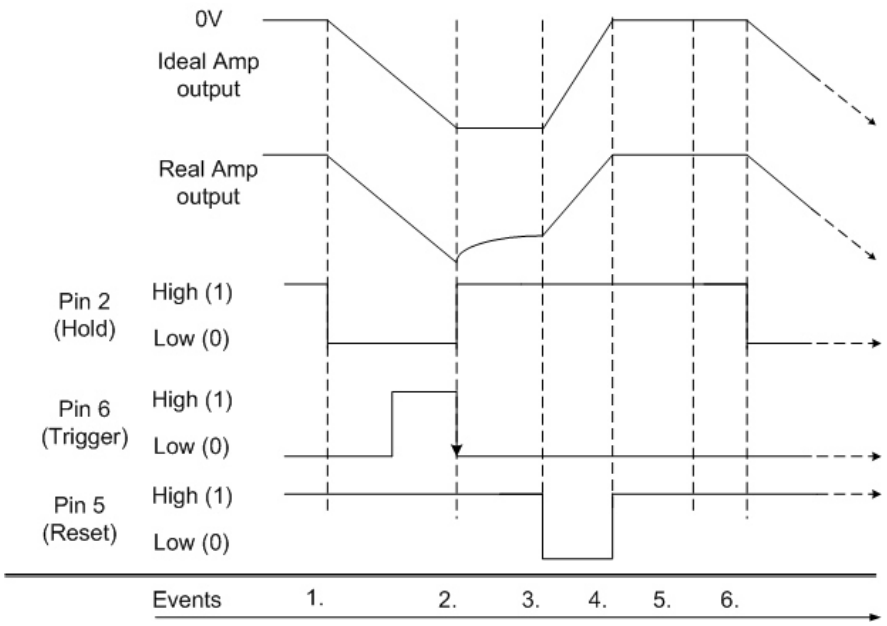

Figure 3.2: Switching sequence layout

The table 3.1 presents the realised parameters of the switching sequence.

Event	Time T in [ms]	Comment
1. to 2.	1 to 1000 ms	Integration time (time to load the capacitor)
2.	$3-5$ ns	Trigger (initialises the measurement of the DMM)
2. to 3.	1 to 300 ms	Hold time (measurement time for the DMM)
3. to 5.	1 to 2 ms	Reset the capacitor
4. to 5.	$3-5$ ns	Hold the 0 Voltage value
5. to 6.	minimal	In the applied case = 0

Table 3.1: Switching characteristics of the integrator

The following figure 3.3 presents the realised measurement sequence with the output voltage in green, the hold sequence in blue and the reset in orange. This plot is taken with the Agilent Technologies MSO9104A oscilloscope with 5 V and 100 ms per division.

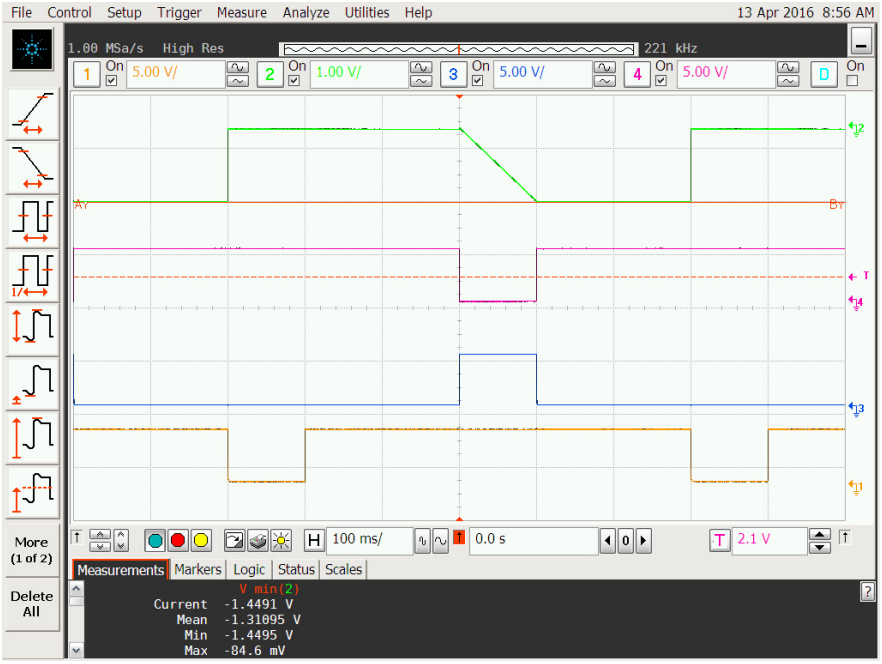

Figure 3.3: Realised switching sequence and voltage output

In order to ensure that the switching signals comply with the required TLL standard, the rise and fall-time was measured for each individual output-pin of the Arduino. The following table shows an average time of $3,8$ nsec to switch from 0 to 5 V. For the reason that the integrated MOSFET switches and the TLL triger are sensitive to the 2 V level it is ensured that the real delay is below $3,8$ nsec (table 3.2).
The stability of the realised sequence impacts the overall stability or precision of the integrator. To ensure the performance of the realised sequence the stability is analysed with the Allan deviation which is presented in the section 4.3.1.

Pin	Rise-time in [nsec]	Fall-time in [nsec]
Pin 2	2,9	3,8
Pin 5	4,2	4,2
Pin 6	3,2	4,4

Table 3.2: Switching performance

The programmed sequence is based on the so called port manipulation method where single ports can be directly addressed on register level. Together with pre-scaling of the 8 bit clock signal the objected minimal time of 1 ms was defined.
To be able to switch two ports synchronously, the timing section in the code was realised with interrupts. Furthermore this interrupts enable to reset the clock register to prevent potential overflow.
The switching sequence was programmed with If statements which count until the condition of the pre-scaled clock signal becomes true.

The simplified logic flow is illustrated in the figure 3.4. The hold, reset and integration time values are defined by the user in order to keep the variables adjustable for the integration to the measurement set up. The hold time depends on the acquisition rate of the DMM. Using a different DMM might need a change in the hold time.
The integration time is implemented as a variable which can used to change the gain of the integrator. The reset time is set to 5 ms (500 μsec are required by the ACF2101BU datasheet) to ensure a stable output voltage of 0 V is reached. The margin of the factor 10 was implemented. In the first stage the clock samples were pre-scaled to 1 ms in order to comply with the objected minimum integration time of 1 ms. In the $2nd$ stage the If condition counts until the target value of the variable is reached and triggers the output action using the port manipulation method. At the end of the cycle the condition is incremented to become 0 in the next step. In addition the realised code is attached to the Appendix A.

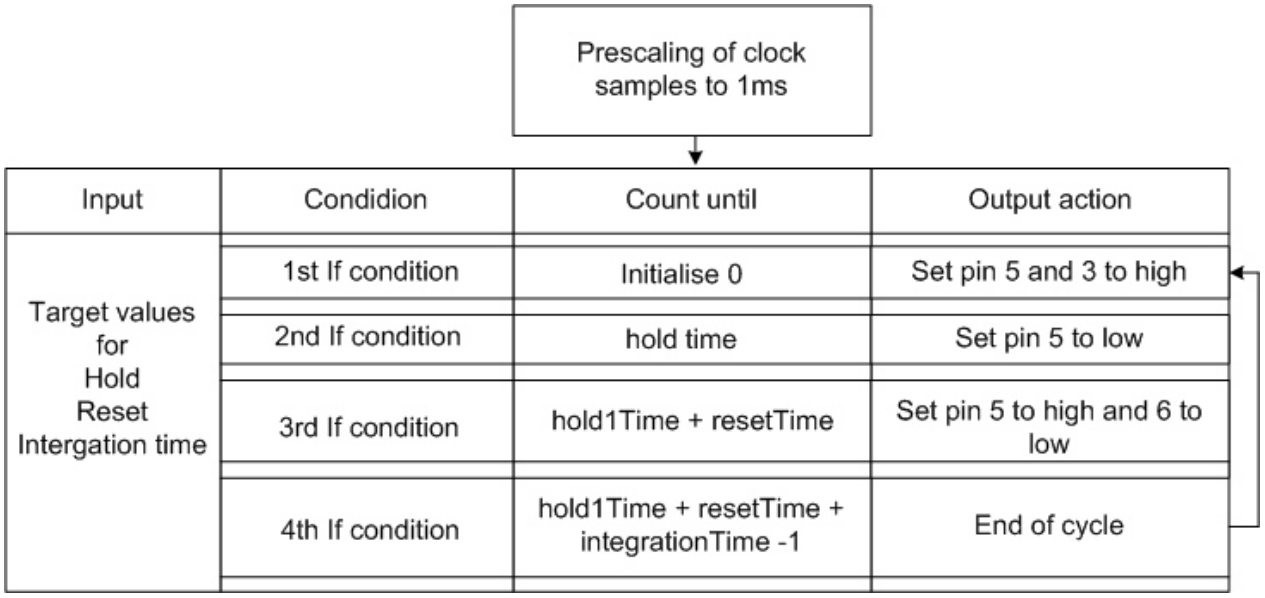

Figure 3.4: General code structure

3.3 Capacitor selection

To select the suitable capacitor type and value an pre investigation with the oscilloscope Agilent MSO9104A was done to analyse the different leakage behaviour of different capacitor types with the same nominal value of 100 pF. For this test the same integrator configuration with the adjusted switching (hold time = 100 ms) sequence was used.

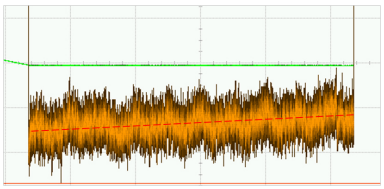

Figure 3.5: Aged (noisy) PTFE capacitor

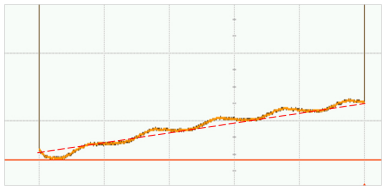

Figure 3.6: Mica capacitor

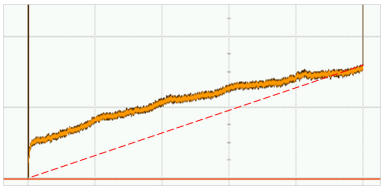

Figure 3.7: NPO ceramics capacitor

With the equation 2.2 the parasitic leakage current can be estimated for the nominal capacitance of 100 pF and 100 ms integration time with the input current of $\sim$ 1 nA. It is possible to see the 50 Hz power-line distortion which is caused by the unshielded 1 MΩ resistor of the reference current source. The figures from 3.5 to 3.7 are taken with a scale of 20 ms and 5 mV per division at the sampling rate of 2 MSa/s. The three capacitor types are presented with the estimated leakage currents in the following table 3.3.

Capacitor	Leakage current
PTFE	$\approx$ 18 pA/100 ms
Mica	$\approx$ 31 pA/100 ms
NPO ceramics	$\approx$ 75 pA/100 ms

Table 3.3: Leakage current estimation for different capacitor types with 100 pF

In order to minimise the leakage current of the available silver-mica capacitor the hold time was minimised to the accessible limitations of the switching capabilities to read and store one sample (below 5 ms). The leakage current for the mica capacitor can be seen as proportional to the hold time so the minimised leakage current was estimated with around $1,55$ pA/5 ms. This estimated leakage current with $\sim 0,8$ % is close to the required precision of 1 % at the 200 pA.

Regarding the capacitor value and integration time the proportional decrease of parasitic effects for higher capacitance was considered and proportionately applied to the low current value of $0,2$ nA. To keep the minimum noise level of the amplifier chip and to balance the capacitor value, integration time, measurement time 5 ms, reset time 1 ms, the frequency of sequences was set to $f_s = 9,35$ Hz in order to enable around $\sim$ 9 readings pre second. To achieve the stability and linearity requirements, the integration time was set to 100 ms and

the capacitance of the silver-mica capacitor value of 100 pF was used up to the maximum output range of $\sim$ 10 V.

3.4 Current source

The reference current source is based on the reference voltage source and a single wire wound resistor with the impedance of 200 $M\Omega$. Applying the Ohm's law the ideal resistor provides 10 nA at 2 V. With a static measurement approach the linearity in form of the relative deviation to the linear regression fit was measured (visual reading of stable digits) with the nano-ampere-meter Keithley 2612. The 200 $M\Omega$ wire-wound resistor with open shielding is presented in figure 3.8.

Figure 3.8: Wire wound resistor with the nominal impedance of 200 $M\Omega$

The following figures (3.9 and 3.10) present a validation regarding the linearity of the wire-wound resistor.

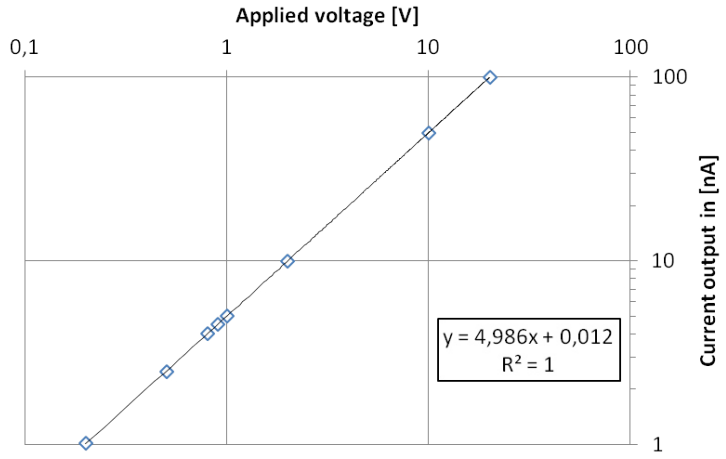

Figure 3.9: Input output relation of the wire wound resistor

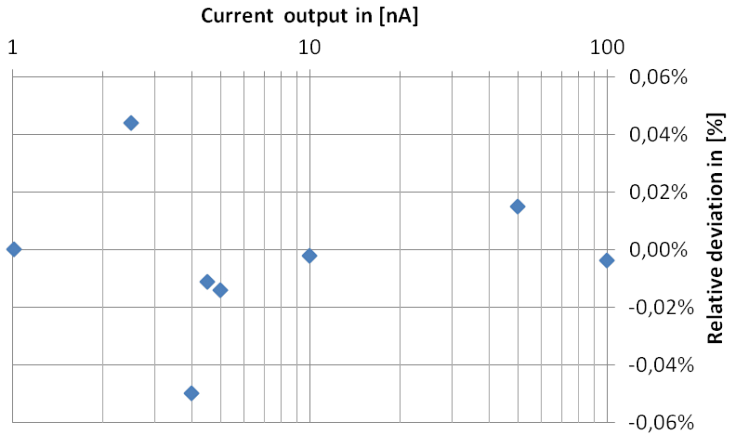

Figure 3.10: Relative deviation of the linearity

3.5 Grounding and shielding

One important aspect of the general design is the shielding and grounding system (figure 3.11). To avoid or minimise the pickup of power line noise at around $\simeq$ 50 Hz a special ground system and shielding was used. The ideal configuration would be a star constellation where all ground connections bundle together.
The design principle was applied to the amplifier and its housing, but in reality it is difficult to avoid the so called ground loops when multiple devices are used. In some cases the housing has a different ground then the shielded cable c_2) and c).

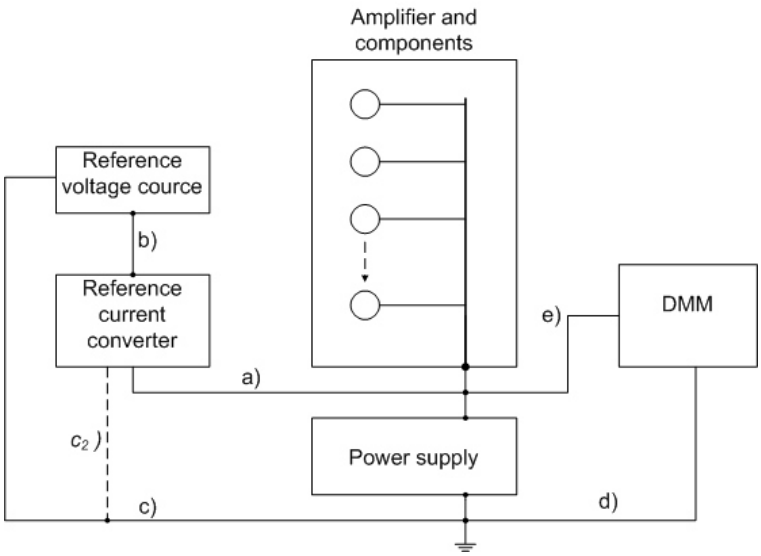

Figure 3.11: Ground system of the experimental set-up

3.6 Realised integrator design

The complete design is based on eight main components which are described below and presented in the following figure 3.12.

1.) The integrator ACF2101 with implemented MOSFET switches.
2.) The BNC connector for the input current with a strait connection to the amplifier input pin (not soldered to the PCB).
3.) Interchangeable integrator capacitor with the suitable terminal is soldered to the required pins.
4.) The copper plated single layer PCB board is the central platform for all ground connections and mountings.
5.) The Arduino platform (Duenilanove) in this particular case where the switching code and serial communication is performed.
6.) The Arduino is powered independently via the serial connection while the amplifier chip is powered by an external voltage source.
7.) The trigger signal output with the BNC connector.
8.) Voltage output of the amplifier provides the output for the digital multi meter.

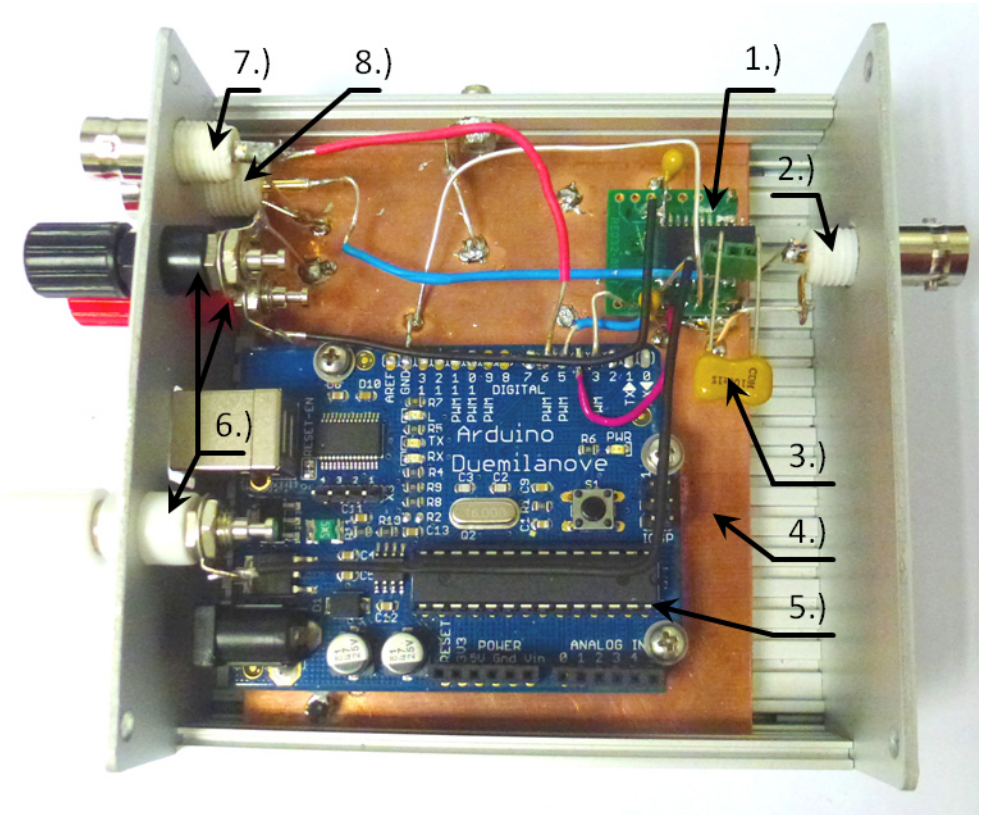

Figure 3.12: Realised integrator configuration

3.6.1 Bill of materials (BOM)

The economical aspect, the cost for one set-up is presented in the following table 3.4. The final sum does not include the BNC cables nor any instrument or soldering equipment.

Component	Cost in Euro
1x ACF2101BU chip	33, 10
1x Interface PCB	5, 60
2x Power supply capacitors 2 nF	0, 28
1x Mica capacitor 100 pF	4, 05
1x Ground plate	4, 93
1x Arduino	20, 24
3x BNC connectors	16, 02
3x Cinch connectors	3, 39
1x Enclosure	15, 00
Wire and shrink tube	1, 00
Solder	1, 00
Sum	104, 16

Table 3.4: Material cost of the set-up

3.7 LabVIEW integration

In order to change the configuration regarding the integration time, the LabVIEW user interface was developed. The main advantage of this configuration is that there is not need to upload the complete adjusted code to Arduino. If there is a change required, the new value will be applied within the following loop by overwriting the existing integration time. The front end (presented in figure 3.13) shows next to the serial communication parameters the trend with previous changes.
Functionality description in context of the block diagram is presented in the appendix B.

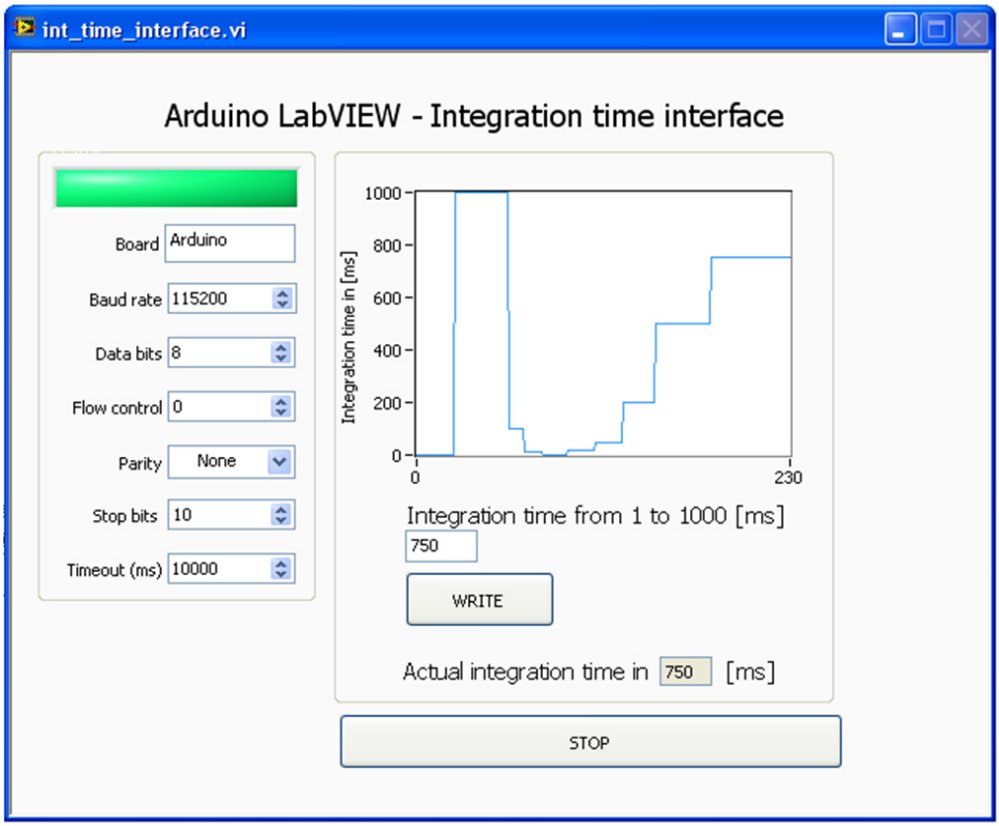

Figure 3.13: LabVIEW interface with serial communication

3.8 Set-up for validation

For validation of the integrator and measurements which are described in the next chapter the following set-up was used (figure 3.14). To generate the most stable current input for the amplifier the calibrator Wavetek 4808 was used in combination with the single resistor configuration as described in the sections 3.4.
The set-up includes the external power supply for the amplifier. The triggered Keysight 34410A with $6\frac{1}{2}$ true digits were used to take one reading per switching cycle.
The measured results from the DMM were transferred directly to the measurement computer with the LabVIEW interface to store each sample. All components were covered by the common ground shielding as described in section 3.5.

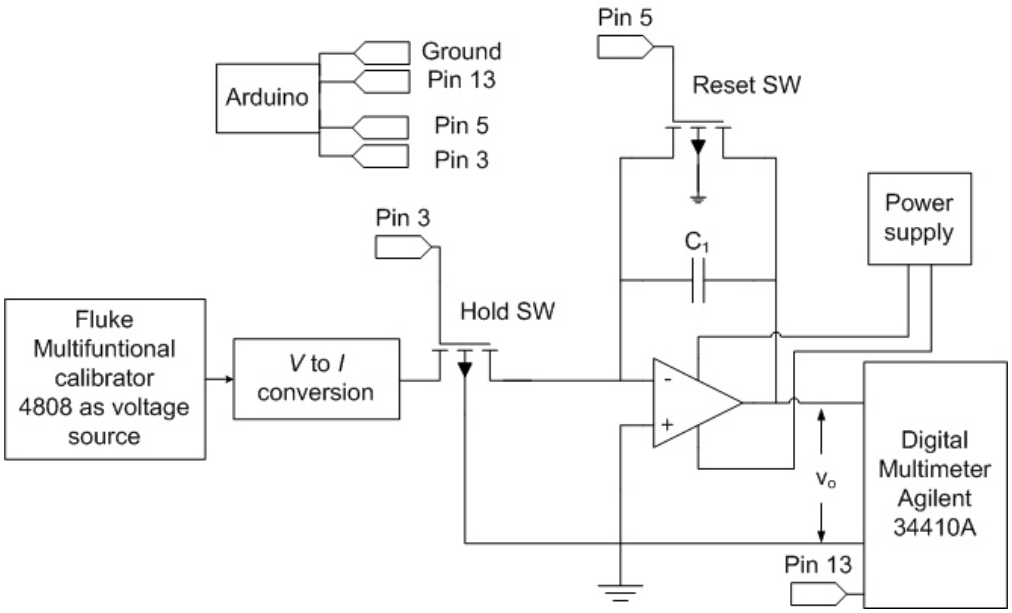

Figure 3.14: Set-up for validation

Chapter 4

Results

Current chapter presents the measurement results that are based on the previously described experimental set-up.
The main focus of the validation was linearity and precision in context of stability and repeatability. In order to choose the suitable statistical methods the measured values were tested for normality. The results are presented in form of the Allan deviation and statistical time series analysis. All tests are conducted under standard laboratory conditions.

4.1 Linearity analysis

To attain the linearity, 10 measurement points were taken into account within the range from $0,2$ nA to 10 nA. Each measurement point represents the mean value of 200 samples, measured at the frequency of $\sim 9,35$ Hz. The following figure 4.1 presents the input output relation. It can be seen that the samples fit to the linear regression.

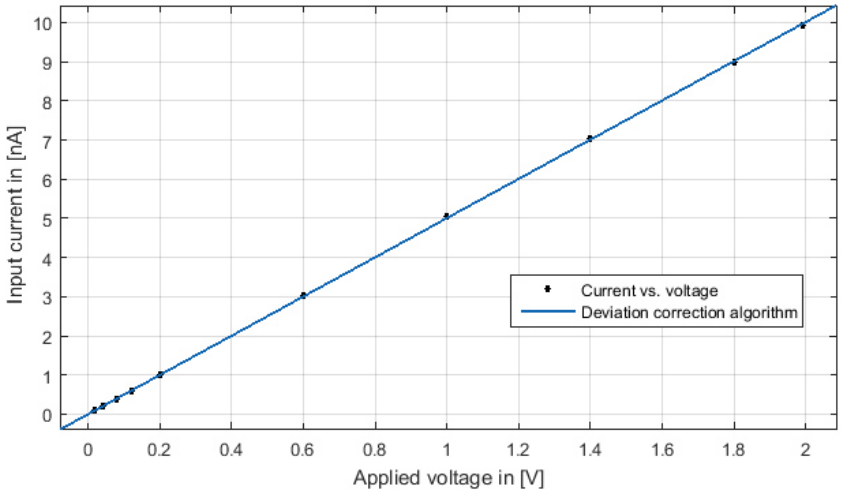

Figure 4.1: Input voltage vs. generated current

The linear equation $f(y) = a * x + c$ was applied to the measured data. The following table

4.1 presents the parameters for the ideal linear reference.

Parameter	Value
a	5.007
c	$7.449e-06$
y	Input current value
SSE	0.002273
R-square	1
RMSE	0.01685

Table 4.1: Linear fit parameters

As the linear regression fit does not show the (small) residuals, the linear regression fit is subtracted by the input current and divided by the input current to get the relative deviation in [%]. The figure 4.2 shows the relative deviation vs. the input current. Except one measurement point (at 1 nA) the general characteristics indicate a strong exponential trend which describes a rising relative deviation with lower current values.

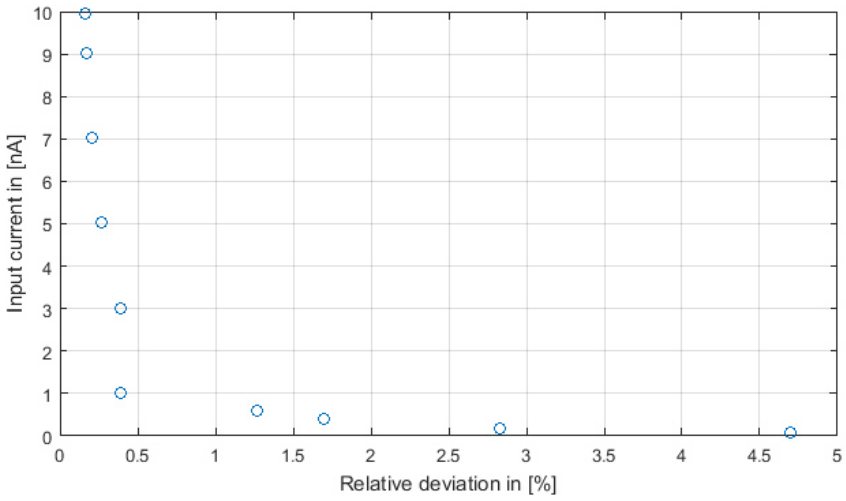

Figure 4.2: Relative deviation vs. input current algorithm

4.1.1 Residual correction algorithm

The exponential increase of the residuals is shown in figure 4.3. Excluding the measurement point at 1 nA the following equation $f(x) = a * x^b$ provided the best approximation. The general form of the approximation is presented in figure 4.3.
In the $1st$ approximation stage the algorithm follows the general characteristics of the exponential function. The parameters of the exponential function are shown in the table 4.2.

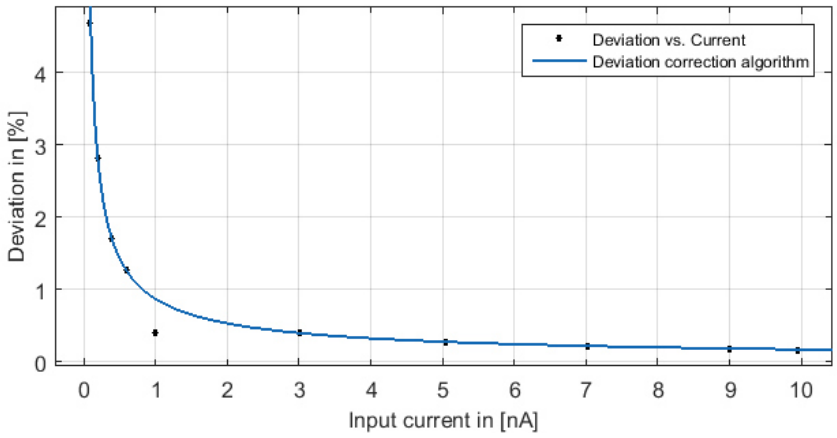

Figure 4.3: Residuals vs. input current with exponential fit

Parameter	Value
a	0.2671
c	-0.733
x	Applied voltage
SSE	0.05436
R-square	0.9973
RMSE	0.08243

Table 4.2: Parameters of the 1*st* stage approximation

Figure 4.4 shows the residuals after the subtraction of the first exponential fit relative to the actual applied current. The relative deviation after the 1*st* stage follows the same exponential characteristics. The maximum deviation at 100 pA after the 1*st* correction stage is clearly below $-0,6$ %. The fitting parameters of the exponential correction algorithm are shown in the following table 4.3.

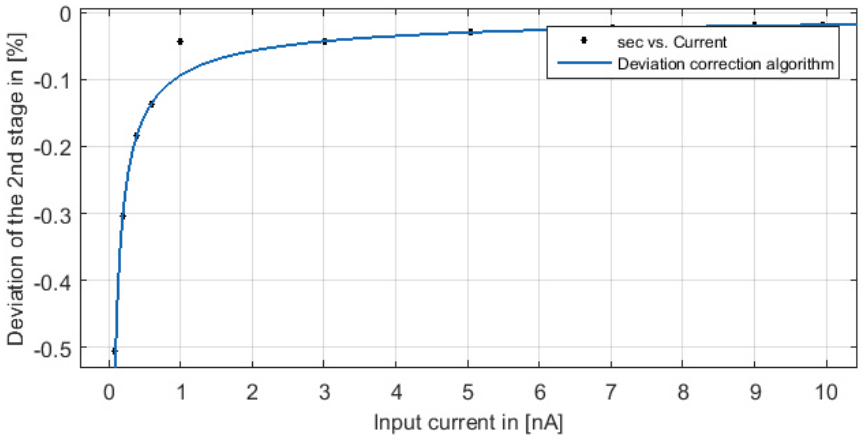

Figure 4.4: Residuals after the 1*st* correction stage

Parameter	Value
a	-0.09357
b	-0.7181
x	Applied voltage
SSE	0.0006795
R-square	0.9971
RMSE	0.009216

Table 4.3: Parameters after the $1nd$ approximation stage

The final corrected relative deviation is presented in figure 4.5. The general exponential characteristic still remains and theoretically a third correction stage could be applied for lower relative deviation. The table 4.4 presents the final parameters of the exponential regression fit.

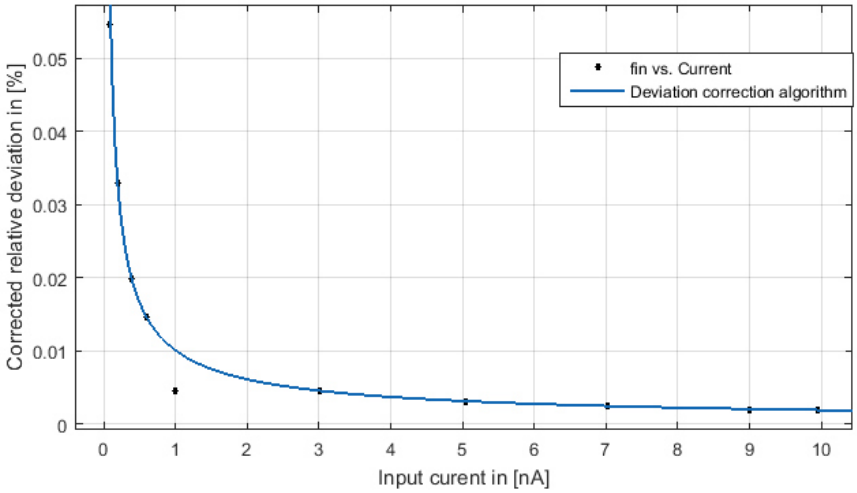

Figure 4.5: Relative deviation after the $2nd$ correction stage

Parameter	Value
a	0.0101
b	-0.7181
x	Applied voltage
SSE	$7.914e-06$
R-square	0.9971
RMSE	0.0009946

Table 4.4: Parameters after the $2nd$ stage approximation

4.2 Test of normality

In order to evaluate the distribution of the measured samples three normality test were chosen to return the test decision if the measured distribution complies with the normal distribution. In order to provide a testable statement the three methods were used for comparison of the p-value.

The histograms, which are presented in the figures below, show the individual distribution of the output voltage at the current input level of $0,1$ nA, 1 nA and 10 nA. The histogram of the input current below 1 nA are based on 10 000 samples while the histogram of the 10 nA input current is based on 200 samples. To validate the distribution the required number of samples is bigger than 20 in each case.

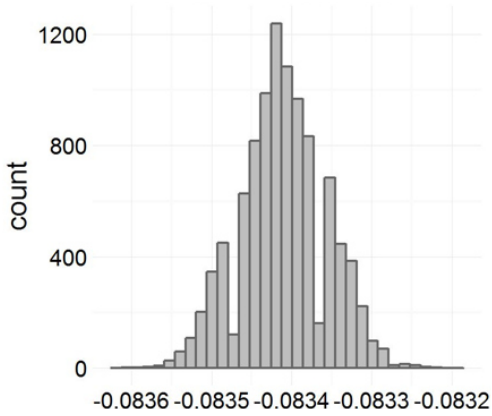

Figure 4.6: Histogram at the input current level of $0,1$ nA.

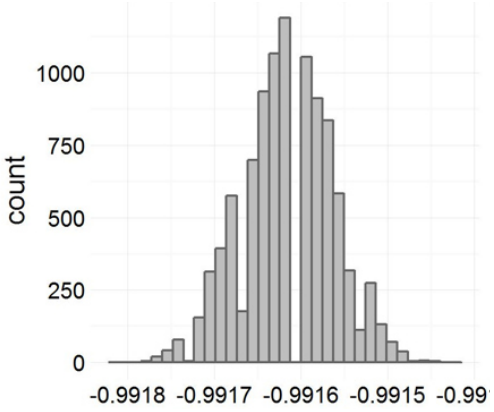

Figure 4.7: Histogram at the input current level at 1 nA.

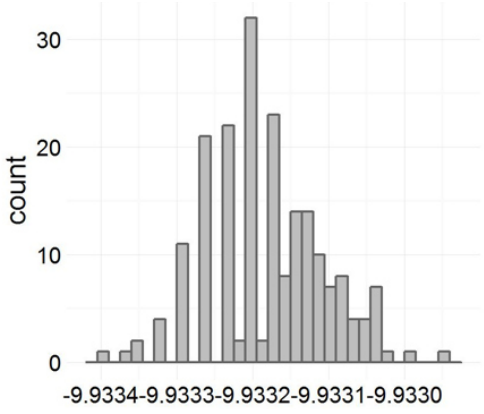

Figure 4.8: Histogram of the integrator output at 10 nA.

The Kolmogorov-Smirnov-test rejects the null hypothesis that the measured data relays on the normal distribution at 5 % significance level (p-value $> 0,05$). The D value represents the maximum of the cumulative fraction difference to the normal distribution.

Kolmogorov-Smirnov-test			
	100 pA	1 nA	10 nA
D	$0,054217$	$0,054246$	$0,065051$
p-value	$< 2,2 * 10^{-16}$	$< 2,2 * 10^{-16}$	$0,03882$

Table 4.5: Outcome of the Kolmogorov-Smirnov-test

The Shapiro-Wilk normality test outcome is the statistical coefficient W and the p-value. The p-value indicates the significance of the Shapiro-Wilk coefficient W and rejects the null hypothesis for 100 pA and 1 nA. For the 10 nA the distribution indicates a high similarity to the normal distribution.

Shapiro-Wilk normality test			
100 pA	14 nA	10 nA	
W	$0,99409$	$0,99373$	$0,99365$
p-value	$1,726 * 10^{-13}$	$5,42 * 10^{-14}$	$0,55$

Table 4.6: Results of the Shapiro-Wilk normality test

The Pearson chi-square normality test rejects the null hypothesis with the p-criteria for all three current input values.

Pearson chi-square normality test			
	100 pA	1 nA	10 nA
X^2	38466	37210	$28,99$
p-value	$< 2,2 * 10^{-16}$	$< 2,2 * 10^{-16}$	$0,01048$

Table 4.7: Summary of the pearson chi-square normality test

4.3 Stability analysis

In order to confirm the stability over period of $\sim$ 18 min, the following results are based on 10 000 samples. The test was performed with the set-up shown in figure 3.8 together with the 100 pF mica capacitor at $\sim 9,35$ Hz sampling frequency under standard laboratory conditions. The stability analysis is prorated into Allan deviation and time series analysis.

4.3.1 Allan deviation

Deviation of the integrator output

To validate the stability of the integrator output signal the Allan deviation shows two noise types which can be identified. White noise can be found from 1 to $\sim$ 200 Time/τ and the floor noise $1/f_{noise}$ starting from $\sim$ 200 Time/τ. The floor noise level begins around $\sim$ 200 Time/τ, starting from this point only marginal improvements in the stability by averaging the measurement samples are possible. The equivalent averaging time to 200 Time/τ is around 22 sec. The maximum floor noise ($1/f_{noise}$) was found to be on the level of $4 * 10^{-6}$ V. Comparing this level with different input current levels (100 pA and 1 nA) it can be seen in figure 4.9 that there is only a marginal difference.

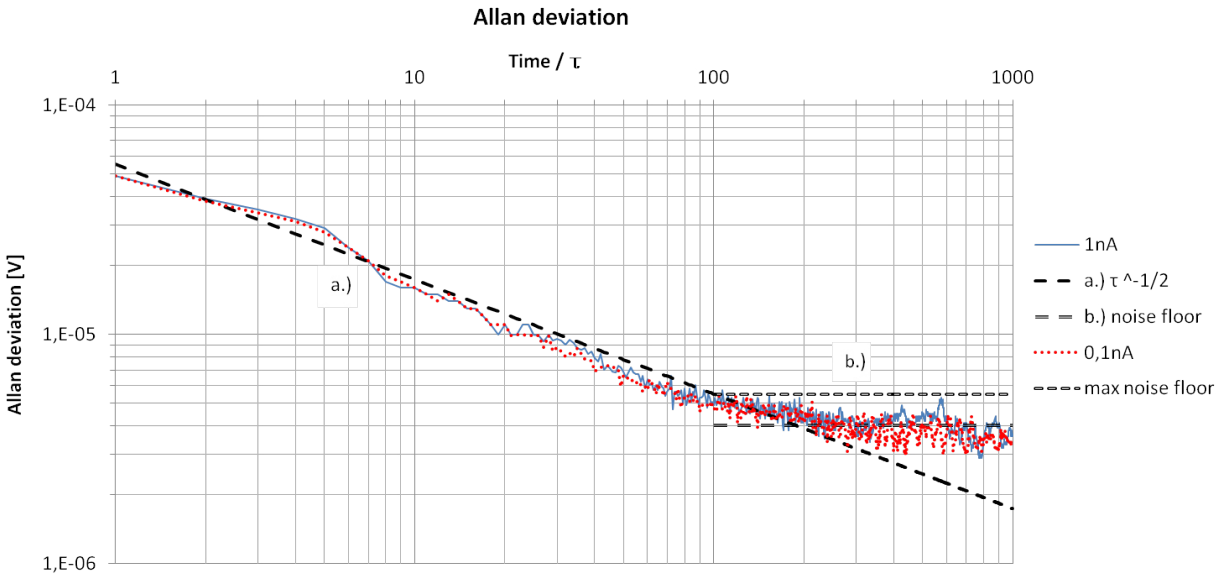

Figure 4.9: Allan deviation at 1 nA and 0, 1 nA current input

Allan deviation of the switching Arduino

To analyse the switching stability of the Arduino the period of 0, 107 sec was measured 10 000 times. The Allan deviation analysis presents the max floor noise ($1/f_{noise}$) level at $1,2 * 10^{-12}$ sec. The averaging time to minimise the implied instability can be found $\sim$ 3 sec.

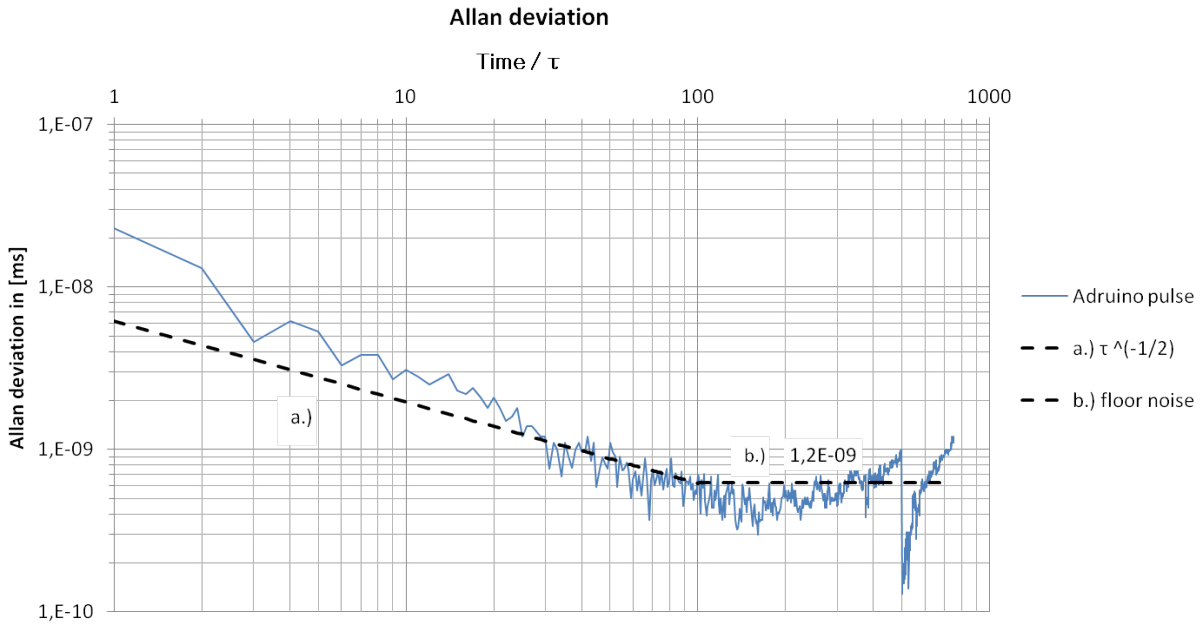

Figure 4.10: Allan deviation of the switching Arduino

4.3.2 Time series analysis

The time series analysis provides the "rest" drift or slope compensation over the measurement time of $\sim$ 18 min. To compensate the drift and offset, the residual analysis method was applied. The drift compensation was based on a linear assumption. The residual analysis was applied in absolute and relative values.

Absolute deviations

The figure 4.11 presents the voltage output of the integrator (at 1 nA input current) over the number of 10 000 samples (measured at $9,35$ Hz). The linear regression fit with the equation $y = 8,9 * 10^{-10} * x - 0,99$ was found. The sub-figure (yellow-trend) presents the residuals based on the linear fit of the measurement data (in blue). The output drift during the experiment can be estimated to be around $0,89$ nV/18 min. Furthermore, the minimum and maximum values of $-0,9912$ V and $-0,9918$ V indicate a high stability level.
The next outcome of the analysis is that the residuals do not significantly vary over time which indicates a very low level of non-linearities. For this configuration with the input current of 1 nA the drift corrected output stability was found to be $-0,99$ V$\pm\ 2 * 10^{-4}$ V.

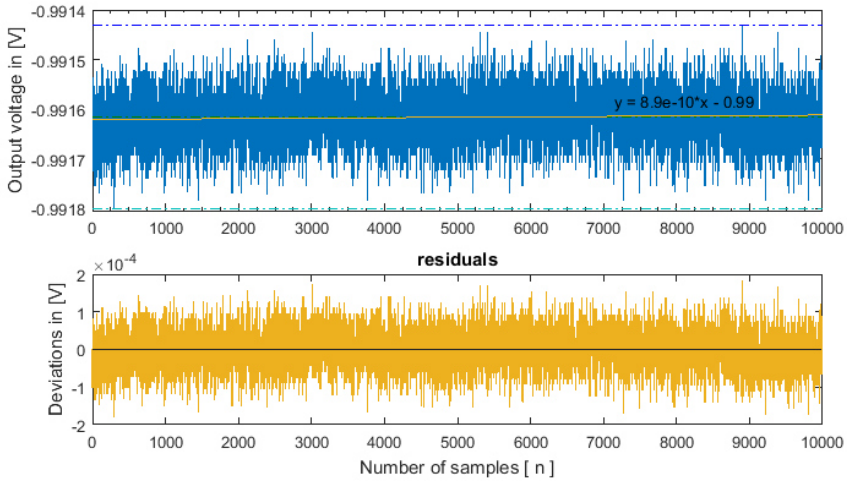

Figure 4.11: Trend for time stability at 10 000 samples at 1 nA

At the level of 100 pA the residual analysis (shown in figure 4.12) with the linear drift compensation follows similar characteristic to the previous analysis at the current level of 1 nA. The linear regression fit indicates a drift of around $4,1$ nA over the full range. The residuals remain below 200 μV with a relative homogeneous noise level. In addition the maximum and minimum values of $-0,0832$ V and $-0,0836$ V indicate a high level of stability at the lowest tested current level. With the residual analysis the stability in absolute values of the integrator output after the drift compensation was found to be $-0,083$ V $\pm 2 * 10^{-4}$ V over the full range.

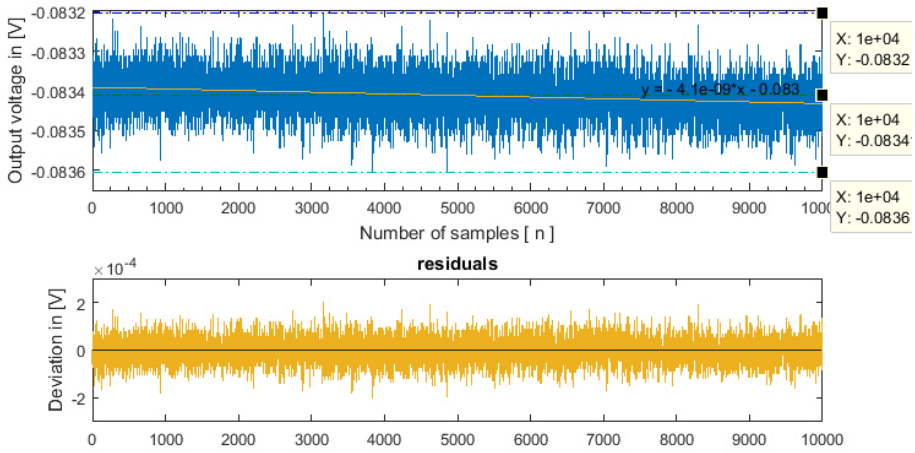

Figure 4.12: Time stability with linear drift compensated deviation at 100 pA

Relative residuals

The relative residual analysis is based on the deviation between the linear regression fit compared to the mean value. The outcome of this analysis represents the relative deviations

over the samples. The analysis is based on the same data sets than the analysis with absolute deviations. The relative deviation in the upper part of figure 4.13 shows some offset which is corrected by the secondary linear regression. The residual analysis presents a stability of $0,16\ \% \pm 0,02\ \%$.

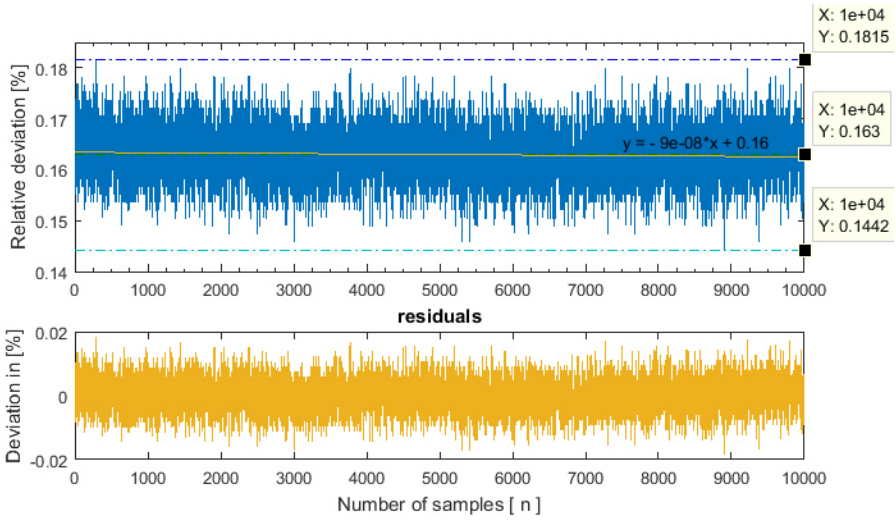

Figure 4.13: Time stability with linear drift compensated deviation at 1 nA

At the input current level of 100 pA the linear regression equation in figure 4.14 shows a relative close range. The residual analysis is, also in this case, based on the linear drift assumption. The results of the relative residual analysis at the level of 100 pA are $0,47\ \% \pm 0,2\ \%$.

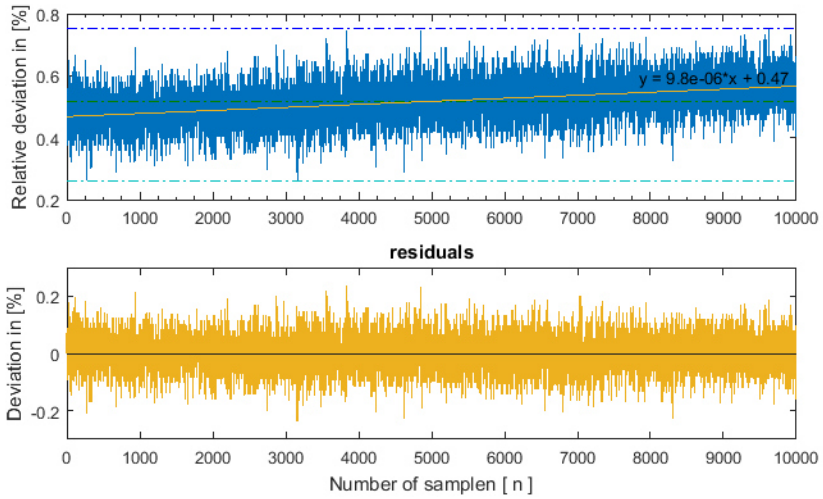

Figure 4.14: Drift compensated relative deviation at 100 pA

Chapter 5

Conclusion

In this chapter the most important findings are presented and compared with the initial objectives. Additionally some suggestions for further research are made.

As it comes to the Allan deviation the $Time/\tau$, the floor noise level and the averaging time show a clear difference between the set-up and the Arduino. To be able to compare the Allan deviation of the two tests, the averaging time to minimise deviations provides the common unit. The switching sequence of the Arduino needs less averaging time (~ 7 times lower) to reach the characteristic floor noise level. Also the noise floor of the Arduino is significantly lower.

The time series analysis provides a $2nd$ approach to analyse the precision in terms of stability and repeatability. The results of the residual analysis for the expected duration time of an experiment 18 min with 10 000 samples show a very stable characteristics. In absolute values the deviations after the drift compensation were found to be at the level of $2 * 10^{-4}$ V. In relative values the variations of the measurements were below $0,5$ % at the input current range of 100 pA.

At the beginning of the thesis three hypothesis were stated. The $1st$ was about the stability of the switching sequence and the influence on the output stability. It was expected that a relative small instabilities in the switching sequence generate a high output instability.
To provide a sequence which was stable enough to switch the MOSFETS of the integrator, a program was developed based on the microcontroller ATmega328P. Several iterations and versions were tested to optimise the performance regarding fast, stable and synchronous switching capability. Those characteristics were needed to minimise offsets, drifts and accumulation of currents before the integration. All these side effects were investigated and minimised to keep the linearity and precision in context of repeatability and stability as high as possible from the very beginning.

The 2*nd* hypothesis looks at the non-linear effects of the set-up and the possibility for compensation. During the linearity analysis of the set-up an exponential relation between the relative deviations for lower input current values was detected. To correct these non linear effects for current values below 1 nA a single therm exponential function together with a bi-square algorithm was used for modelling and compensation.

The 3*rd* hypothesis is connected with the stability of the current source, general parasitic effects, shielding against power line noise and their expected influence on precision and linearity. The stability of the current source was discovered with a settling characteristic. This effect was found to have a great impact on all measurement results in general. Other parasitic effects like leakage currents of different capacitor types were investigated and evaluated for the timing sequence. The power line noise even under laboratory conditions was detected. The shielding cover was integrated into the ground system to minimise the interference as much as possible.

Recommendations for future work:

The real boundaries of the integrator in context of the low current input and gain limitations are not found jet. The quality of the measured signal indicates that lower current values can be measured.
The dynamic limitations of this set-up are not part of this thesis. Results show that there can be room for higher sampling rates. In case of lower input current ranges or higher frequency it might be beneficial to use commercial available PTFE capacitors to minimise the leakage currents.

Chapter 6

Summary

The digital multimeter Agilent 3458A which is used at Metrosert AS presently has a limited low current measurement capability; it does not measure current values below 100 nA. The goal of this Master's thesis was to design and validate a switched integrator with high gain to convert low current levels precisely into voltage. The required input current range of the switched integrator was set to be between 200 pA and 10 nA. The main criterion for validation were the linearity and precision in context of repeatability and stability.

In order to understand the behaviour of the ideal and the real integrator and the current source, a model with the related differential equations was developed. Three methods (were introduced which) are used for comparing the similarity of the measurement samples distributions to the normal distribution. With these methods it is possible to choose a suitable approach for further analysis. In the present thesis Allan deviation and time based residual analysis were preferred. Additionally, to get an impression of the expected power intensity, the input and output relations of the integrator were estimated together with a chosen photodiode.

The experimental part presents the programmed microcontroller which was used to generate the switching sequences for the integrator. To provide a stable switching sequences, a program was developed with synchronous switching capabilities. The program is based on registers and port manipulation methods which are triggered by the pre-scaled clock signal of the Arduino.
In order to choose the most suitable capacitor type for the integrator, three capacitor types were compared. The base for comparison were their individual leakage current characteristics. The best performance (of those commercially available capacitors at the time) had the silver-mica capacitor with the nominal value of 100 pF.
Before the integration of individual components, the suitable ground system was designed. Several possible integration aspects were considered, for example short signal paths and the

avoidance ground loops. To be able to change the integration time without uploading new code to the Ardoino a LabVIEW interface with serial communication was developed and implemented into the switching sequence loop.

The measurements were made with an output of a voltage reference calibrator and a single high quality 200 MΩ resistor. The current source generated a stable input signal for the integrator validation. With this pre-validated current source, the experiments for linearity and precision in context of stability and repeatability were performed. The linearity was obtained by the manual adjustment of the calibrator and by measuring the voltage output at the same time with a triggered digital multimeter. The linearity analysis is based on 10 points over the required range and 200 samples at one single point have been taken. After the linearity test two exponential correction algorithms were developed and applied in two stages. The relative deviation after the correction was below $0,06$ % at the input current of 100 pA.
In order to test the integrator regarding its precision in context of stability and repeatability, 10 000 samples were taken at the current levels of 100 pA and 1 nA at the frequency level of $9,35$ Hz.
To choose the suitable methods for further analysis the measurement samples were tested regarding their similarity to the normal distribution. For this test three different statistical methods were applied. The 5 % criteria for the similarity to the normal distribution was not reached, so the measurement results were not normal distributed.
To investigate the characteristic floor noise level, the Allan deviation was applied to the measurement samples of the integrator output and to the Arduino switching sequence. The characteristic floor noise level at the input current of 100 pA and 1 nA were found to be similar. In both cases the maximum floor noise level of $4 * 10^{-6}$ V was found. Comparing the averaging time between the switching sequence and the integrator output it can be stated that the noise contribution of the switching sequence was factor ~ 7 lower than the integrator set-up.
For further repeatability analysis of the same data set with 10 000 samples ($\sim$18 min), the time based residual analysis was used to get the drift corrected deviations in absolute and relative values. For the input current level of 100 pA the output of the integrator was measured and a linear drift compensation was applied. The stability at the input current level of 100 pA was found with $-0,083 \pm 2 * 10^{-4}$ V over the duration time of 18 min. The relative residual analysis presented a deviation of $0,47\% \pm 0,2\%$ at the same input current level. At the current level of $1n$ A the results improved in absolute values to $-0,99$ V $\pm 2 * 10^{-4}$ V and in relative values to $0,16 \pm 0,02$ %.

The outcome in general is better than required. The results match the expected behaviour of

an exponential increase of deviations with lower current values. The corrected linearity was found to be lower than 1 %. The precision in terms of stability and repeatability, including the drift correction, was found to be lower than $0,5$ % at the input current level of 100 pA. Compared to the required 1 % deviation at the current level of 200 pA, the realised integrator performed better than required.

Kokkuvõte

Digitaalsel multimeetril Agilent 3458A, mida hetkel Metrosert AS-is kasutatakse, on piiratud võimalused; see ei mõõda väärtusi alla 1 nA. Käesoleva magistritöö eesmärk oli disainida ja kinnitada võimas lülitiga integraator, millega saaks madala voolutaseme täpselt voltidesse teisendada. Vajaminev lülitatud integraatori sisendvool oli seatud 200 pA ja 10 nA vahele. Peamine valideerimise kriteerium oli kordusvõime ja stabiilsuse lineaarsus ning täpsus.

Selleks et ideaalse ja tõelise integraatori ja vooluallika käitumist mõista, loodi seotud diferentsiaalvõrranditega mudel. Tutvustati kolme meetodit, mida kasutatakse mõõtenäitude jaotuste ja normaalse jaotuse sarnasuste võrdlemiseks. Nende meetoditega saab edasiseks analüüsiks valida sobiva lähenemisviisi. Käesolevas töös eelistati Allani deviatsiooni meetodit ja ajapõhist residuaalset analüüsi. Et saada aimu oodatavast võimsuse intensiivsusest, hinnati lisaks ka integraatori sisendi ja väljundi suhet koos valitud fotodioodiga.

Eksperimentaalne osa tutvustab programmeeritud mikrokontrollerit, mida kasutati integraatori lülitusjadade genereerimiseks. Et võimaldada stabiilset lülituste jada, arendati sünkroonse lülitamisvõimega programm. Programm põhineb registritel ja portide manipulatsiooni meetoditel, mille päästab valla eelmõõdetud Arduino kellasignaal. Sobivat tüüpi kondensaatori valimiseks võrreldi kolme tüüpi kondensaatorit. Võrdluse põhjaks võeti nende individuaalse lekkevoolu omadused. Kõige paremini esines (hetkel saadaolevatest mudelitest) hõbe-vilgu kondensaator nominaalväärtusega 100 pF. Enne individuaalsete osade kokkupanekut loodi sobiv alussüsteem. Arvestati mitmeid võimalikke kokkupaneku aspekte, näiteks lühikesed signaalahelad ja maandussõlmede vältimine. Et muuta integratsiooniaega ilma Ardoinosse uut koodi üleslaadimata, arendati ja kaasati lülitamisjadasse LabVIEW liides koos jadaandmesidega.

Mõõtmed võeti pinge kalibraatori väljundi ja ühe kõrgekvaliteetse 200M takistiga. Vooluallikas genereeris integraatori valideerimiseks stabiilset sisendsignaali. Eelvalideeritud

vooluallikaga viidi läbi stabiilsuse ja kordusvõime lineaarsuse ja täpsuse katsed. Lineaarsus saavutati kalibraatori manuaalse kohendamise ja samaaegselt digitaalse multimeetriga pinge väljundi mõõtmise läbi. Lineaarsuse analüüs põhineb kümnel punktil nõutud vahemikus, ühes punktis võeti 200 mõõdet. Pärast lineaarsuse teste arendati kaks eksponentsiaalset parandusalgoritmi, mida rakendati kahes staadiumis. Pärast parandusi oli suhteline hälve 100 pA sisendvoolu juures alla $0,06$ %. Selleks et testida integraatori stabiilsuse ja kordusvõime täpsust, võeti 10 000 mõõdet 100 pA ja 1 nA voolu ja $9,35$ Hz sageduse juures. Et edasiseks analüüsiks sobivaid meetodeid valida, testiti mõõteid nende normaalse jaotuse põhjal. Selleks rakendati kolme erinevat statistikameetodit. Normaalse jaotuse sarnasusega võrdlemisel ei jõutud 5 % kriteeriumini, st mõõtmised ei jagunenud normaalselt.
Minimaalse müra taseme omaduste uurimiseks rakendati integraatori väljundi ja Arduino lülitijada mõõtenäitudele Allani hälbe meetodit. Müra tase leiti nii 100 pA kui ka
1 nA suuruse sisendi juures olevat sarnane. Mõlemal juhul oli maksimaalne müra tase $4 * 10^6$ V. Võrreldes keskmist aega lülitijada ja integraatori väljundi vahel, võib öelda, et lülitijada müra panus oli integraatori ülesseadmisest 7 madalam. Sama 10 000 mõõtenäidu (18 min) edasiseks kordusvõime analüüsiks, kasutati ajapõhist residuaalanalüüsi, et saada absoluutsete ja relatiivsete väärtuse kõrvalekaldega korrigeeritud hälved. 100 pA sisendvoolu juures mõõdeti integraatori väljundit ja rakendati lineaarset kõrvalekalde tasakaalustamist. 18 minutilise aja jooksul leiti 100 pA sisendvoolu stabiilsus olevat $0,083$ V $\pm$ $2 * 10^4$ V. Suhteline residuaalanalüüs andis sama sisendvoolu juures hälbeks $0,47$ V $\pm$ $0,2$ %. 1 nA suuruse voolutugevuse juures tulemused paranesid absoluutväïrtustes $0,99$ V $\pm$ $2 * 10^4$ V ja relatiivväärtustes $0,16$ % $\pm$ $0,02$ %.

Tulemused vastavad madalate voolutugevuste hälvete eksponentsiaalse suurenemise oodatud käitumisele. Magistritöö tulemusel valminud integraatori mõõtmistulemused ületavad täpsuselt töö alguses seatud eesmärke. Korrigeeritud lineaarsus leiti olevat madalam kui
1 %. Stabiilsuse ja kordusvõime täpsus, sh kõrvalekalde parandused, leiti olevat madalam kui $0,5$ % võrreldes nõutud 1 % 100 pA sisendvoolu juures, kui on nõutud 200 pA voolutugevus.

Appendix A

Arduino uno code

```
int timer1_counter;
int count = 0;
byte bMask;
byte dMask;
byte dMask2;
byte dMask3;

int hold1Time = 200;
int resetTime = 100;
int hold2Time = 200;
int integrationTime = 100;
int readchintegrationTime;

void setup()
{
Serial.begin(115200); //enable serial communication
randomSeed(analogRead(0));

  DDRD = B00001000; //set ports of pin 3 and 5 to high B00101000
  DDRB = B01000000; //set port of pin 13 high B01000000

  dMask = B00001000; //pin3
  dMask2= B00100000; //pin5
  dMask3= B01000000; //pin6
  bMask = B00100000; //pin13

  // initialize timer1
```

```
  noInterrupts();           // disable all interrupts
  TCCR1A = 0; //set timers to 0
  TCCR1B = 0;

  timer1_counter = 65286;  /// preload timer 65536-16MHz/64/1000Hz

  TCNT1 = timer1_counter;   // preload timer
  //TCCR1B |= (1 << CS12);    // 256 prescaler
  TCCR1B |= (1 << CS10); //64
  TCCR1B |= (1 << CS11);
  TIMSK1 |= (1 << TOIE1);   // enable timer overflow interrupt
  interrupts();
}

ISR(TIMER1_OVF_vect) // interrupt service routine
{
  TCNT1 = timer1_counter; // preload timer

  if(count == 0) // initiliye cycle
  {
    PORTD = dMask; // pin 3 high/ pin6 low
    PORTD |= dMask2; // pin 5 high
  }
  if(count == hold1Time) // hold 1 time passed
  {
    PORTD &= ~dMask2; // pin 5 low
  }
  if(count == hold1Time + resetTime) // hold 1 and reset time passed
  {
    PORTD |= dMask2; // pin 5 high
  }
  if(count == hold1Time + resetTime + hold2Time) // hold 1, reset, hold2 time passed. St
  {
    PORTD &= ~dMask; //pin 3 low
    PORTD |= dMask3; //pin 6 high
  }
  if(count == hold1Time + resetTime + hold2Time + integrationTime -1) // cycle ended
  {
```

```
    count = -1;
  }

  count++; // increment counter each timer tick
}
void loop()
{ if (Serial.available())
{ readintegrationTime = Serial.parseInt();
//read the ch1High value from LabView}
integrationTime = readchintegrationTime;
Serial.println (integrationTime);//write the ch1High value to LabView
delay(150); //Delay to transmit the written value
}
```

Appendix B

LabVIEW interface

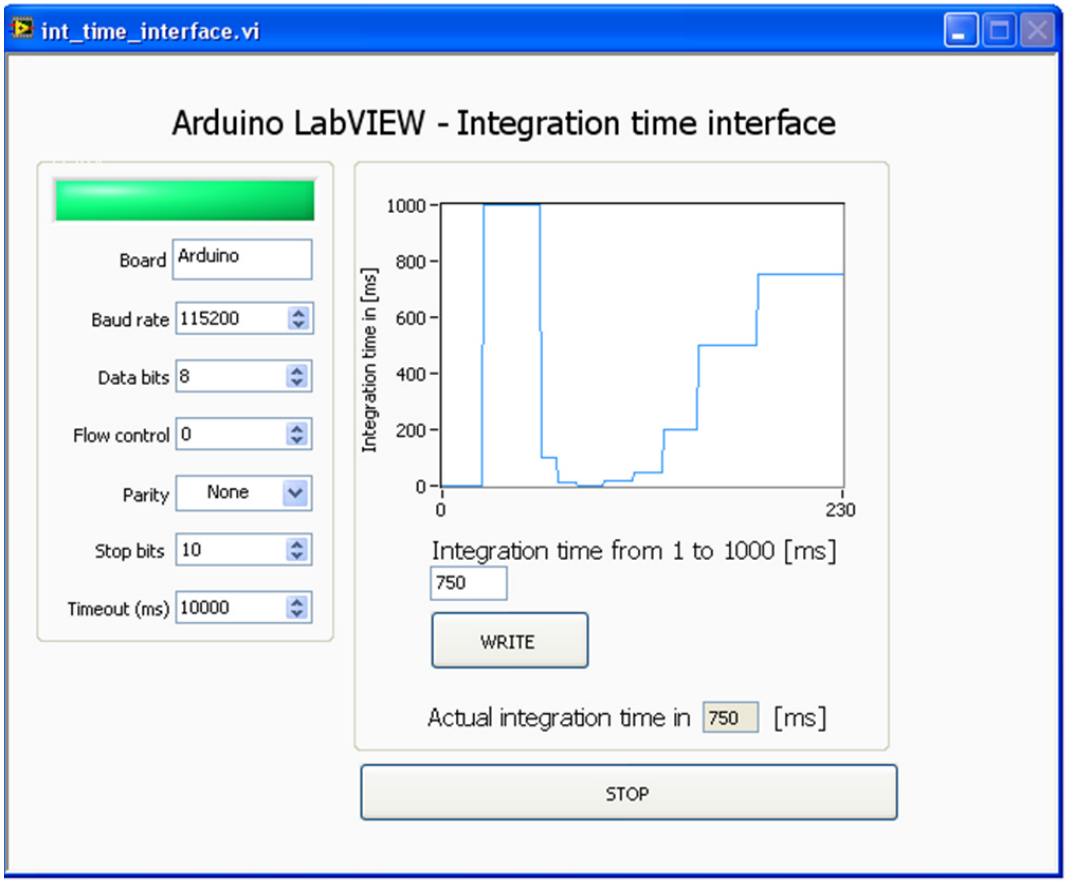

Figure B.1: LabVIEW front end

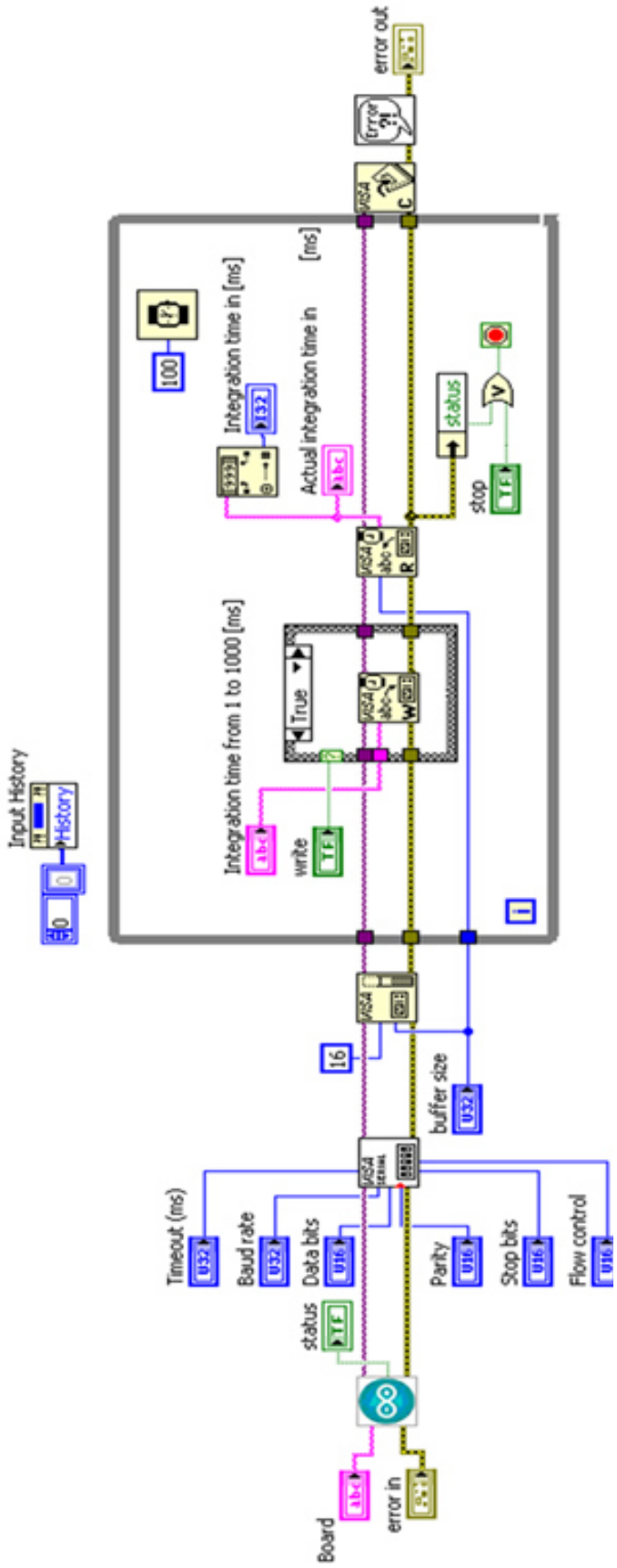

Figure B.2: LabVIEW block schematics for serial communication

Bibliography

[1] A. Agarwal and Jeffrey H. Lang. Foundation of Analog and Digital Electronic Circuits. *Elsevier Inc.* p.729, 2005.

[2] V. Aggarwal, Meng Mao and Una-May OReilly. A Self-Tuning Analog Proportional-Integral-Derivative (PID) Controller. *IEEE Computer Society* First Conference on Adaptive Hardware and Systems, 2006.

[3] E. Benkler, Christian Lisdat, Uwe Sterr. On the relation between uncertainties of weighted frequency averages and the various types of Allan deviations. *Physikalisch-Technische Bundesanstalt*, Germany , 2015.

[4] M. De Groot, M. Schervisch. Probability and Statistics. *Pearson Education, Inc.*, 4th edition p.698 - 707, 2012.

[5] W. Guggenbühl, T. Loeliger, M. Uster, F. Grogg. CMOS Circuit for low photocurrent measuremnts. *Electronics Laboratory, Swiss Federal Institute of Technology, Zürich, Switzerland*, 1:1–6, 1996.

[6] S. Guinta. The applications Engineer-21. *http://www.analog.com/library/analogDialogue /Anniversary/21.html*, 1:1-6, last time opened at 20.04.2016.

[7] Hamamatsu Photonics. Datasheet S1337 series. *SI photodiodes* p.1-6, 2016.

[8] M. Johnson. Photodetection and Measurement, maximizing performance in optical systems. *McGraw-Hill*,:p.83, 2003.

[9] P. Kadkhoda, L. Jensen, D. Ristau Facility for fast Mapping of Total Scattering and Transmission in the Spectral Range from DUV- NIR. *SPIE*, Vol. 9628:96280N-4, 2015.

[10] H. Liu, Purnendu K. Dasgupata and Hong J. Zheng. High performance optical absorbance detectors based on low noise switched integrators. *Tantala*, 7:1331–1338, 1993.

[11] J. Mountford, Geiland Prrovecchio, Marek Smid and Radiskav Smid. Developement of a switched integrator amplifier for high-accuracy optican measurements. *Applied Optics*, 47(31), 2008.

[12] J. Ofloff. Introduction to Probability and Statistics. *MIT course 18.05.* readings 16-19, 2014.

[13] S. Park, Kee-Suk Hong, and Wan-Seop Kim. Switched integration amplifier-based photocurrent meter for accurate spectral responsivity measurement of photometers. *Applied optics*,Vol. 55:Nr.9, 2016.

[14] Texas Instruments. Datasheet ACF2101. *original from Burr Brown* p.1-16, 2010.

[15] H. Thode. Testing for normality. *Marcel Dekker, Inc.* readings 3-19, 2002.

List of Figures

List of Tables